European Journal of Remote Sensing

ISSN: 2279-7254 (Online) Journal homepage: www.tandfonline.com/journals/tejr20

Shrub height estimation for habitat conservation in NW Iberian Peninsula (Spain) using UAV LiDAR point clouds

P. Rodríguez Dorribo, C. Alonso Rego & R. A. Díaz Varela

To cite this article: P. Rodríguez Dorribo, C. Alonso Rego & R. A. Díaz Varela (2025) Shrub height estimation for habitat conservation in NW Iberian Peninsula (Spain) using UAV LiDAR point clouds, European Journal of Remote Sensing, 58:1, 2438626, DOI: 10.1080/22797254.2024.2438626

To link to this article: https://doi.org/10.1080/22797254.2024.2438626

Published online: 16 Dec 2024.

EUROPEAN JOURNAL OF REMOTE SENSING
2025, VOL. 58, NO. 1, 2438626
https://doi.org/10.1080/22797254.2024.2438626

Shrub height estimation for habitat conservation in NW Iberian Peninsula (Spain) using UAV LiDAR point clouds

P. Rodríguez Dorribo [a], C. Alonso Rego [b] and R. A. Díaz Varela [a]

[a]GI-1809-BioAplic, Departamento de Botánica, Escola Politécnica Superior de Enxeñaría, Campus Terra, Universidade da Santiago de Compostela, Lugo, Spain; [b]Departamento de Ingeniería Agroforestal, Escola Politécnica Superior de Enxeñaría, Lugo, Spain

ABSTRACT

This study aimed to develop and validate a method of estimating 3D parameters from DJI Zenmuse L1 LiDAR on DJI Matrice 300 RTK UAV data to characterise and monitor the structure and conservation status of dense shrub formations. The shrub heights were estimated using Progressive Morphological Filter (PMF) and the *Ground Filter* module of the FUSION/LDV software. A digital terrain model (DTM) was interpolated with RMSE 0.23 and 0.27 m, respectively, and a normalised canopy height model (nCHM) was calculated by subtracting it from the LiDAR data and the best DTM obtained. The reliability of the estimates was evaluated against georeferenced field data. In addition, the study examined the impact of vegetation characteristics and return reduction in the original point cloud on the accuracy of LiDAR-data derived . Significant differences were found in the correlations between observed and estimated data for the DTM ($R^2 = 0.9998$) and nCHM heights ($R^2 = 0.51/0.54$). The corresponding RMSE values were 0.23 and 0.34 m. Moreover, no significant differences in the reliability were found for different vegetation types, whereas reduction point cloud density (up to 25–50 returns/m^2) did not significantly affect accuracy. In conclusion, lightweight UAV LiDAR can effectively detect sub-metric scale vegetation 3D structure, useful for fine-scale habitat conservation.

ARTICLE HISTORY
Received 29 May 2024
Revised 22 October 2024
Accepted 2 December 2024

KEYWORDS
LiDAR; UAS; Digital Terrain Model; canopy height model; shrubland height; DJI Zenmuse L1

Introduction

Shrub formations make up 44% of the forest cover in Spain («Bosques españoles y su evolución», s. f.), playing an essential role in the functioning and provision of ecosystem services. Human intervention and recurrent fires have contributed to the expansion of shrubland. This type of ecosystem generally occupies degraded land in harsh environments or land subjected to management regimes that hamper the establishment of forest cover. In addition, some shrub formations accumulate large amounts of biomass and their ecosystems play an important role in biodiversity conservation, and they are catalogued as habitats of community interest in the Natura 2000 network of protected areas in Europe (DECRETO 37/2014 polo que se declaran zonas especiais de conservación os lugares de importancia comunitaria de Galicia e se aproba o Plan director da Rede Natura 2000 de Galicia 2014) Processes related to global changes, such as climate change, intensification or abandonment of agrarian activities represent a threat to the conservation of these habitats (Petrou, Manakos, y Stathaki 2015). For all the above reasons, studying, characterizing, monitoring, and managing shrub formations are of vital importance. The design of effective conservation measures for this type of habitat requires robust data on habitat structure and function. As these habitats are often extensive (occupying wide areas, even in landscapes that tend towards fragmentation and mixed land cover in areas that are strongly affected by anthropogenic activity), the use of remote sensing is recommended because of the associated advantages regarding the systematic, spatially explicit data acquisition and the high benefit–cost ratio for large areas (Reddy, 2021; Turner et al., 2003).

LiDAR (light detection and ranging) sensors have been successfully used in vegetated area research in recent years (Kaartinen et al., 2012; Guerra-Hernández et al., 2021, 2017; Deng et al., 2023; Fu, Zhang, et al. 2024b) LiDAR technology determines the distance between an object and the sensor by measuring the time taken between emission of pulsed light waves of known characteristics and return of the pulses to the sensor after interacting with the ground and other biophysical objects. Combined with precise information about the position of the sensor and a ground referencing system, the technology provides a cloud of georeferenced points containing accurate height data. LiDAR estimates 3D structures better than traditional inventory and mapping techniques, including photogrammetric systems, because of the

CONTACT P. Rodríguez Dorribo patricia.rodriguez.dorribo@usc.es GI-1809-BioAplic, Departamento de Botánica, Universidade de Santiago de Compostela, Escola Politécnica Superior de Enxeñaría, Benigno Ledo, Lugo 27002, Spain

capacity of the pulses to penetrate vegetation cover (Dandois et al., 2015; E. P. Baltsavias, 1999a). For this reason, the technology is gradually being adopted as the preferred method for generating canopy height models (CHMs) and Digital Terrain Models (DTMs) (Meng et al., 2010). Additionally, as LiDAR is an active sensing system, it is not strongly dependent on weather or light conditions. It therefore improves work performance, with simpler data processing, less effort, and fewer limitations regarding capture of data used to generate DTMs, and it also enables characterization of vegetation layers at previously unknown levels of detail and precision (Kellner et al., 2019).

Both airborne laser scanning (ALS) and terrestrial laser scanning (TLS) techniques are particularly suitable for analysing the spatial and dynamic characteristics of forest cover, including tree and understorey layers, thus helping to clarify the role of these layers in the biosphere (Rowell et al., 2015). However, the high cost of ALS, which is far superior to other existing techniques, limits its use in small areas or when the flights must be repeated in zones where poor results have been obtained (Hartley et al., 2020). On the other hand, although TLS provides a source of accurate, detailed data and performs better in smaller areas than ALS, large inputs of time and effort may be required to acquire the data, especially in complex areas such as tropical forests and dense shrub formations (Brede et al., 2017; Wilkes et al., 2017). Some researchers have therefore questioned whether remote scanning techniques will replace traditional plot inventories (Liang et al., 2016).

The possibility of using LiDAR systems in unmanned aerial vehicles (UAVs) (from now onward unmanned laser scanning – ULS) has recently opened up a new way of working that could solve the problems related to measuring the height of vegetation, by providing good mobility and rapid data acquisition. This confirms that the technique is an attractive tool for forestry studies (Liang et al., 2019; Novo et al., 2020).

Various authors have compared the performance of the ULS technique with those of TLS, ALS, and structure from motion photogrammetry (SfM) in forest environments (mainly tree stands) with promising results (Brede et al., 2017; Hartley et al., 2020; Liang et al., 2019; Wieser et al., 2016; Zaque et al., 2017). Comparison of the performance of ULS and UAV-SfM for height measurement in young plantations yielded R^2 values of 0.99 and 0.94 and a RMSE value 0.15 and 0.48 m respectively (Hartley et al., 2020). Related results were obtained for conifers, with $R^2 = 0.95$ and RMSE = 6.47% (Jaakkola et al., 2017), and for *Eucalyptus globulus* Labill, with RMSE = 0,52 m (Wallace et al., 2014). Likewise, comparison of ULS and TLS showed that although TLS provided more accurate estimates for most forest metrics, except height, the results obtained by ULS were reported to be similar, considering the advantages of the embedded LiDAR (Liang et al., 2019). Finally, in a comparison between ALS and ULS, the latter displayed a lower tendency to underestimate heights (Wieser et al., 2016).

Extensive validation of LiDAR technology has been conducted in the framework of vegetated area research (Hartley et al., 2020; Novo et al., 2020). Recent studies involving tree stands have evaluated the use of ULS for detecting individual trees (Fernández-Álvarez et al., 2019; Kellner et al., 2019), estimating aboveground biomass (AGB) (Dandois et al., 2015; Hartley et al., 2022; Kellner et al., 2019), tree heights and checking the accuracy of DTMs (Liang et al., 2019) and the applicability of various regression models in estimating mangrove tree heights using machine learning (Fu, Jiang, et al., 2024a). Most recent studies involving shrub formations have focused on fire management and estimation of AGB (Dandois et al., 2015; Novo et al., 2020; Rego et al., 2020; Warkentin et al., 2020), although some studies have analysed height underestimation in aerial LiDAR systems (Wieser et al., 2016) or the function of shrub formations as carbon sinks (Fernández-Guisuraga et al., 2022). Analysis of herbaceous vegetation was evaluated in (Miura et al., 2018) and (Streutker & Glenn, 2006).

Vegetation height is one of the metrics most used to validate LiDAR in forest ecosystems. The method usually used to estimate height from LiDAR data consists of subtracting the DTM from the digital surface model (DSM), thus producing the normalised canopy height model (nCHM), which gives the height above ground of each point in the point cloud (Novo et al., 2020). Hence, various authors have indicated the importance of having an accurate DTM for estimating heights and volume from LiDAR data (Estornell, Ruiz, et al., 2011a; Su & Bork, 2006), particularly in shrub areas – where the small distance between the vegetation and the ground may lead to underestimation of the height of the vegetation (Riaño et al., 2007; Streutker & Glenn, 2006)- and in steeply sloping areas (Raber et al., 2002). Several factors, such as the data characteristics, flight altitude, point density, number of returns, footprint size and scanning angle, also affect the accuracy of DTMs (Ahokas et al., 2003; Hopkinson, 2007; Hyyppä et al., 2005; Liu & Zhang, 2008) and height estimation (Hartley et al., 2020; Roussel et al., 2017; E.P. Baltsavias, 1999b).

Recent advances in the miniaturization of LiDAR systems for UAVs, as well as their simplification and consequent reduction in price together make LiDAR technology an innovative option of great interest in forestry (Li et al., 2020; Torresan et al., 2017; Wallace et al., 2012). However, the optimal flight parameters for ULS, such as field of view, flight altitude, velocity and overlap between flight lines, have not yet been established (Liang et al., 2019). Furthermore, the difficulty in producing DTMs from LiDAR data may lead to substantial errors, therefore the possible sources of

error must be identified so that these can be reduced to acceptable levels, particularly in complex environments with dense vegetation and steep slopes (Zhang et al., 2016).

For all of the above reasons, validation of this technology, which would enable its posterior integration with digital photogrammetric data in monitoring studies and shrub management, would represent an asset for monitoring programmes, particularly in generating reliable DTMs for areas of dense vegetation cover, in comparison to monitoring systems based only on fieldwork or RGB photogrammetric techniques, which are of limited use for this type of vegetation. In this regard, cost-effective methods for dense scrub 3D structure measurement might detect encroachment/overgrazing events, assess wildfire risks linked to biomass accumulation, deviation from biodiversity habitat quality baselines and in general support management, conservation and, as in our case, habitat restoration. To the best of our knowledge, there are few studies addressing the study of dense and high scrublands from very high-resolution ULS for biodiversity conservation, being more frequent the use of low-cost SfM for this task (see e.g (Fraser et al., 2016; Klouček et al., 2022).) or manned airborne LiDAR (Estornell, Ruiz, et al., 2011b). The performance and very high resolution ULS might overcome some of the inherent problems in the estimation of vegetation 3D variables in these scenarios, such as the difficulty in field surveys, the high weight of relatively small errors over the low values of vegetation height or the patched pattern that these formations might show depending on the management and environments, among others.

The overall aim of this study was to design and validate a ULS-based method of evaluating vegetation structure, as well as to establish the optimal workflow and determine any possible improvements in field data collection and point cloud processing in steeply sloping areas and dense woody shrub formations predominated by legumes and heaths in the genera *Ulex, Erica* and *Calluna*. More specifically, the study aimed to evaluate the accuracy of a DTM generated from LiDAR data, using non-destructive samples and of heights derived from ULS data for characterizing this type of vegetation. The study also aimed to identify the vegetation height thresholds or differences in the structure of vegetation cover from which the data can be predicted with greatest accuracy, as well as the density of points that enable simplification of the original point cloud without loss of accuracy.

Material and methods

Study area

The study area is located in the Serra do Xistral, in the municipality of O Valadouro, Lugo, NW Spain (Figure 1). Climate is predominantly oceanic, with high rainfall and fogs evenly distributed throughout the year and a mild thermal regime. The Regional potential vegetation is oak or mixed deciduous forests, but wind-exposed hyper-humid slopes at higher altitudes were hardly tree-colonised; rather, they are covered by open wetlands like complex mosaics of acidic mires (blanket and raised bogs) and wet heathlands, whereas on less wet and exposed locations, formations of serial dry heathlands and scrublands occurs (Sevillano et al., 2001). The gradual abandonment of traditional activities, conversion of bog and heath habitats into artificial grasslands and reforestation with fast-growing species such as pines and eucalyptus has led to a level of transformation that threatens habitats of great conservation value, including different types of shrub formations. In the specific case of the study area, the poor livestock distribution related to changes in land use has caused loss of soil due to overgrazing in some zones, and the encroachment of species such as gorse (*Ulex europeus*, *U. galli*) in others due to the abandonment of extensive grazing practices (Blanco Arias et al., 2018). In addition to the large loss of the floristic biodiversity, the shrub formations contain large accumulations of combustible biomass, with the associated risk of severe wildfire.

The object of study was a pilot plot included in a project financed by the LIFE programme, the European Union's funding instrument, "LIFE IN COMMON LAND (LICL) https://lifeincommonland.eu/. The plot, of surface area 13.10 ha, is surrounded by an enclosure made from wood and wire. With the aim of evaluating the effect that grazing by Galician wild horses has on controlling the spread of *Ulex* spp., paths were cleared in 2019 to allow movement of livestock through the plot; the paths cross the plot in a grid-like pattern following the contour lines and maximum slope.

The study area has a mean elevation of 566 m above sea level, ranging from 489 to 682 m. The slope gradient, as per the FAO classification[1] (UN, 2009), is predominantly steep and very steep, averaging 34%. Moreover, the vegetation mainly consists of dense shrub of *Ulex* spp. with the presence of large amounts of ferns in the lower lying areas, thinned areas and cleared strips. Bramble is also present, together with diverse herbaceous species, in the lower and intermediate layers, and heaths/heathers are scarce in

[1](0–2%) – Flat to very gently sloping; (2–5%) – Gently sloping; (5–10%) – Sloping; (10–15%) – Strongly sloping; (15–30%) – Moderately steep; (30–60%) – Steep; (> 60%) – Very steep.

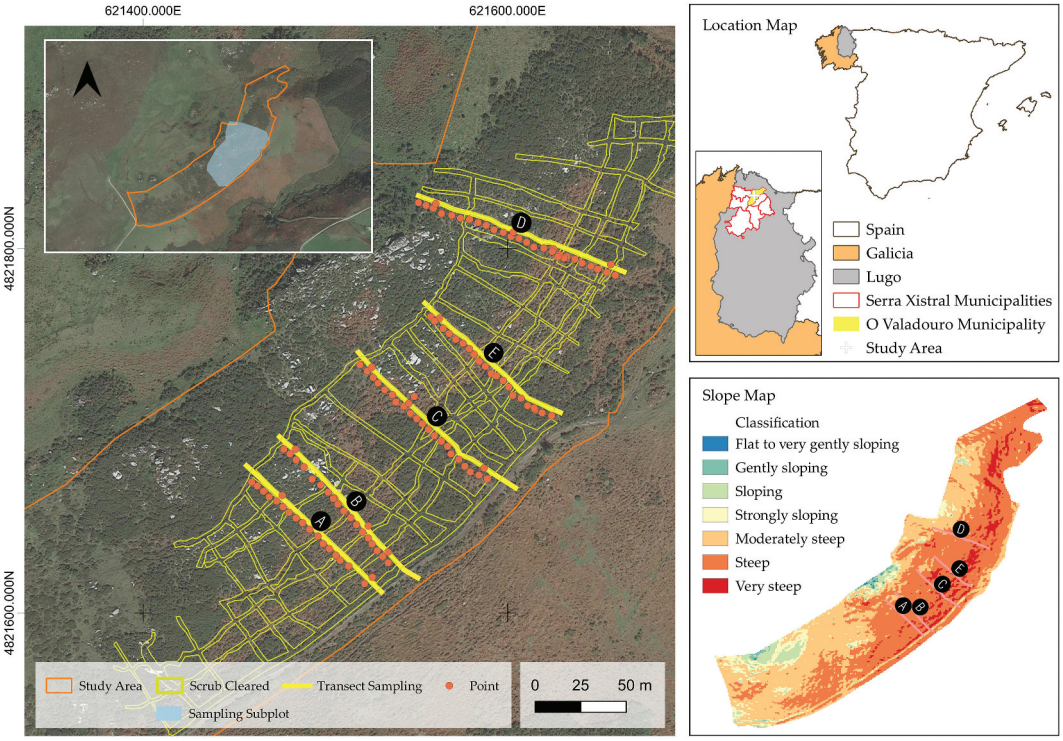

Figure 1. Study area: location, orthophotograph and slope map indicating the sampling points/transects and cleared strips in the experimental plot. Basemaps from https://centrodedescargas.cnig.es/.

coverage. Consisting of plant remains, moss and stems, a highly compacted woody layer of approximate thickness 7 cm can be seen in the litter of the gorse areas.

Data collection

Field inventory

The field data were acquired between 13 and 15 July 2022 by a team of two researchers. The fieldwork planning was based on a non-destructive sampling method, aligning series of points (thereafter transects) along the maximum slope and parallel to existing paths. To mitigate edge effects, these transects were shifted 1–1.5 m within the shrub, perpendicular to the path axis. The number of transects was arbitrarily set at five, and the transects were distributed across the whole plot as a compromise between the resources available and the measurement of a sufficient number of sampling points. Along these transects, systematic point sampling was carried out at regular intervals of 5 m. These sampling points were located along the transects with a laser distance meter (Leica DISTO D8) of accuracy ±1 mm according to the manufacturer. To prevent large deviations in the line, a base cartographic archive was used, with *a priori* location of the beginning and end points for each transect loaded in the GNSS RTK. A total of 119 sampling points were measured in the 5 transects, and the sampling size was considered sufficient to represent the conditions of the shrub vegetation in the plot (Figure 1).

The following data were obtained at each sampling point:

- Sampling point code and location, measured with a GNSS receiver (Trimble R2 GNSS RTK/PPK). The mean vertical accuracy of the sampling points was 0.019 m in the 0.014–0.051 m range, where 75% of the points are below 0.021 m.
- Maximum height of the vegetation above the ground within a radius of 10 cm from the point calculated in the office, when necessary and measured with a graduated ranging pole.
- Visual estimation of vegetation cover around the sampling point (approximately one metre from the point in the direction of the vegetation). The density of the vegetation was established in three categories: high-density gorse cover, low-density gorse cover, no gorse present.
- Species present.
- Height of the dead biomass (litter) layer immediately above the soil.
- The measuring point was photographed during measurement with the ranging pole to record the entire process.

LiDAR data

The LiDAR data acquisition flights were conducted on 13 July 2022, between 11:00 and 14:30 h, in clear conditions with a wind of speed less than 5 km/h. The flights were carried out by the University of Santiago de Compostela's Spin-off 3Edata, and the data were acquired with LiDAR ZENMUSE L1 sensor mounted on a MATRICE 300 RTK platform, both from DJI (Figure 2). The combination of these two instruments provided a maximum horizontal and vertical precision of 10 cm and 5 cm, respectively, for flights of at least 50 m on the object, according to the manufacturer (DJI, 2021). Similar values were obtained in real test surveys carried out by (Acre Surveying Solutions, dir, 2021).

For data capture, two independent flights were carried out at, respectively, 100 and 80 m above ground level (AGL), with a field of view (FOV) of 70.4°/4.5° in repeated mode, and 7 m/s speed. Flight planning and execution were controlled by UgCS Version 4.10.8 software (SHP *Engineering*, Riga, Latvia) and the data captured by the LiDAR sensor were converted to LAS format and projected in ETRS89/UTM Zona 29N – EPSG:25829 coordinate system with elevations referred to the EGM08 ellipsoid, consistent with the GNSS RTK field inventory measurements. LAS files included the X, Y, Z coordinates, up to 3 returns per pulse[2] and intensity coded in 8 bits [0–255]. The values of the parameters and the LiDAR data for each flight are shown in Table 1.

Data processing

The workflow is summarised in Figure 3. Data visualization and processing were conducted using the QGIS 3.22.1 and RStudio free access software (R Core Team, 2022), mainly with the lidR (Roussel et al., 2020; 2023) and rFUSION (Plowright, 2017) packages, along with the FUSION/LDV software. The general work procedure for each flight altitude was based on five steps: ground point classification or filtering; construction of the DTM; height normalization to produce the (nCHM), calculation of the vegetation height for a given cell size; and statistical analysis and validation of the LiDAR data by comparison with georeferenced field data. Different parameters and algorithms were tested at each of these steps, and the choice of the best performing conditioned the next step. With the aim of evaluating their influence on the final results, the characteristics of the vegetation cover were also included in the analysis. In addition, considering the complexities of storage and handling data from high-density LiDAR sensors (Liu & Zhang, 2008), the precision of different point densities was analysed by randomly sampling the original densities at lower reference values (200, 150,100, 75, 50, 25, 10, 5 and 1 points/m^2), based on previously established procedures (Anderson et al., 2006; Liu & Zhang, 2008; Zhao et al., 2022).

Ground point filtering was conducted using the P*rogressive Morphological Filtering* (PMF) algorithm in the R package *lidR* (Roussel et al., 2020;) which implements a modification of the method described by K. Zhang et al. (2003) (Zhang et al., 2003), and the *Ground Filter* module of the FUSION/LDV software adapted from Kraus and Pfeifer (Kraus & Pfeifer, 1998; Plowright, 2017). Both algorithms are frequently used in vegetation analysis and are compatible with the free access software utilized in this study. For each case, the following parameters were used:

Figure 2. LiDAR and GNSS-RTK equipment used in the study.

Table 1. Parameters for data capture by ULS and the point cloud obtained.

Altitude (m)	Line spacing (m)	Pulse frequency (kHz)	N. º of returns (ud)	Speed (m/s)	Density (points/m^2)	1st Return (%)
80	55 (*overlap 40%*)	160	3	7	407.75	98.9%
100	43 (*overlap 66%*)	160	3	7	513.67	99.3%

[2]In this document, whenever points are referred to, they correspond to returns, thus differentiating them from pulses (a single pulse can return up to 3 returns with the equipment used).

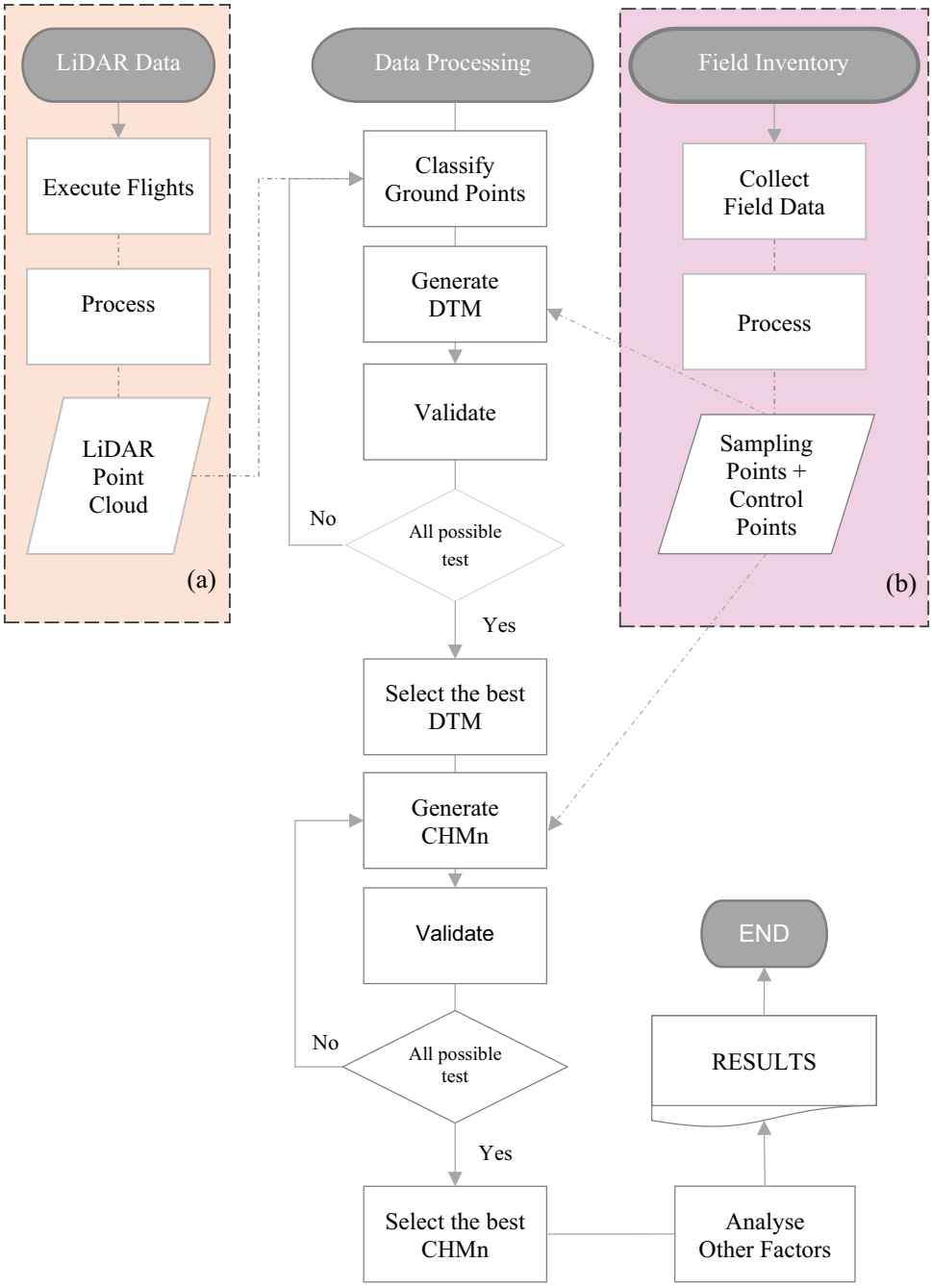

Figure 3. Workflow diagram outlining the data processing steps, including (a) obtaining the point cloud and (b) obtaining the sampling points.

- PMF Algorithm, based on previous experiences (Estornell et al. 2011a), was evaluated using the interactions between window sizes (w0, w1, w2) and four height thresholds (1, 2, 3, 4) as shown in Table 2.
- For Ground Filter Algorithm were used the default parameters *aparam* = 1; *bparam* = 4; *gparam* = −2, *wparam* = 2.5 with 5 iterations, testing the performance for cell sizes of 10.00, 7.50, 5.00, 2.50, 1.00 and 0.50 m.

Table 2. Input parameters in the PMF algorithm.

Window size (m)	Height thresholds (m)			
	1	2	3	4
w0 (1, 2, 3, 4)	(0.1–0.5)	(0.1–1.5)	(1.5–0.1)	(2.5–1.5)
w1 (2, 4, 6, 8)	(0.1–0.5)	(0.1–1.5)	(1.5–0.1)	(2.5–1.5)
w2 (3, 6, 9, 12)	(0.1–0.5)	(0.1–1.5)	(1.5–0.1)	(2.5–1.5)

The ground points obtained in the previous step were used to construct the DTM using the Inverse Distance Weighting (IDW) interpolation technique. IDW is best adapted to areas of dense shrub and is also valid for slopes greater than 15° (Su & Bork, 2006). This algorithm, which is included in the lidR (*knnidw*) library, was used to analyse the performance for resolutions of 0.10, 0.25, 0.5 and 1 m. The DTM accuracy was evaluated using the 119 points used for georeferencing the sampling points.

The normalized heights (i.e. the vegetation height) were calculated by subtracting the previously obtained DTM from the original point cloud (Fernández-Álvarez et al., 2019; Hartley et al., 2022; Miura et al., 2018; Novo et al., 2020). Raster CHM were then calculated from the normalised heights by the *dsmtin* algorithm from the lidR library for pixel sizes of 0.10 and 0.25 m and bilinear interpolation of the maximum height points. In this step, the results were validated against the field measurements of the vegetation height at the 119 sampling points along the transects.

The type of vegetation and density of cover were then analysed as factors potentially influencing the results obtained with LiDAR sensors. The slope, although steep, was rather homogeneous and was therefore not considered. The relative heterogeneity of the density and shape of vegetation cover (and also the height) enables (at least theoretically) the analysis of the influence of such variables on the accuracy of the DTM (Evans & Hudak, 2007; Meng et al., 2010; Su & Bork, 2006). Two factors were established for this purpose: density of cover and shrub height. The categories of vegetation cover and their characteristics are listed in Table 3 for each of these factors.

Model evaluation (validation)

In addition to the standard accuracy statistical measures (estimated vs. measured means, standard deviations, etc.), the reliability of the estimates was evaluated using the coefficient of determination (R^2), the root mean square error (RMSE), the percentage RMSE (RMSE%) and the average model bias (AMB) for the observed data (Díaz-Varela et al., 2018). These were calculated as follows:

$$R^2 = 1 - \frac{\sum_i (\hat{y}_i - \bar{y})^2}{\sum_i (y - \bar{y})^2} \quad (1)$$

$$RMSE = \sqrt{\frac{\sum_{i=0}^{n} (\hat{y}_i - y_i)^2}{n-1}} \quad (2)$$

$$RMSE\% = 100\left(RMSE/\bar{y}\right) \quad (3)$$

$$AMB = \frac{\sum_i (\hat{y}_i - y_i)}{n} \quad (4)$$

where the observed data (measured in the traditional inventory) are represented by *yi*; the estimates (LiDAR data) are represented by $\hat{y}_i$; $\bar{y}$ corresponds to the mean of the observed values, and n is the sample size.

The analysis was completed with Normalized Median Absolute Deviation (NMAD), a robust metric which is an estimate of the standard deviation resilient to outliers in the error distribution (Baltensweiler et al., 2017; Höhle & Höhle, 2009)

$$NMAD = 1.4826 \times median_j \times \left(\left|\Delta h_j - m_{\Delta h}\right|\right) \quad (5)$$

Where:

$median_j$: median of j validation samples.

Δh_j: individual errors of the j validation samples.

$m_{\Delta h}$: median of the errors of the j validation samples.

The effect of the influence of the mediating factors on the absolute error was determined from the absolute error (AE) and the relative error expressed as a percentage (PE) using the following expressions:

$$AE = \left|yi - \hat{y}_i\right| \quad (6)$$

$$PE = \frac{AE}{yi} \times 100 \quad (7)$$

In addition, the results obtained were validated with the F statistic obtained in an ANOVA and which is calculated by dividing the model sum of squares by the residual sum of squares.

Table 3. Categories of vegetation cover for the density and height factors in the study zone.

COVER CHARACTERISTICS		
Code	Category	Description
NG	No gorse present	Regardless of the percentage vegetation cover, there is no gorse present. Vegetation mainly consists of ferns.
HD	High density of gorse cover	The soil and the lower area are not visible, and the gorse occurs as dense compact bushes
LD	Low density of gorse cover	The lower area is visible, but the soil is not always visible, and the gorse occurs as individual branching shrubs.
HEIGHT (h)		
1	≤0.5 m	Vegetation height intervals measured in the field
2	0.5 < h ≤1.0 m	
3	1.0 < h ≤1.5 m	
4	1.5 < h ≤2.0 m	
5	2.0 < h ≤2.5 m	
6	>2.5 m	

$$F = \frac{\sum_{i=1}^{n} (\hat{y}_i - y)^2 / 1}{\sum_{i=1}^{n} (yi - \widehat{yi})^2 / (n-2)} \quad (8)$$

The null hypothesis for this test assumes equal means, while the alternative hypothesis considers differences among them. The non-significant outcome involves performing the TOSTER package's *equ_ftest* function, which statistically determines the equivalence by computing the partial eta-squared (η_p^2) (Caldwell, 2022; Campbell & Gustafson, 2021; Lakens, 2017).

Results

Digital terrain Model

The best result for the DTM (RMSE = 0.23 m, R^2 = 0.9998) was obtained with the PMF algorithm, although there was no significant difference relative to the *Ground Filter* algorithm (RMSE = 0.271 m, R^2 = 0.9998) (Table 4[3]). As can be seen in Figure 4 the PMF parameters that yielded the best results corresponded to a window size w2 at constant intervals of 3 m and a height threshold 1 (range 0.1 to 0.5 m) although with scant difference relative to a threshold 2 (range 0.1 to

Table 4. Accuracy statistics for the Z coordinate (DTM) estimation.

Algorithm	Flight	Mean	SD	Skew	Kurtosis	AMB (m)	R^2	RMSE (m)	RMSE (%)	NMAD (m)
Observed	Z	564,1	14,8	−0,152	−1,051					
PMF	80 m	562,7	14,8	−0,174	−1,047	−1,39	1.0	0.250	0.04	0.211
	100 m	562,8	14,8	−0,168	−1,042	−1,37	1.0	0.230	0.04	0.203
Ground Filter	80 m	562,9	14,8	−0,166	−1,046	−1.20	1.0	0.273	0.05	0.259
	100 m	563,0	14,8	−0,168	−1,039	−1.17	1.0	0.271	0.05	0.279

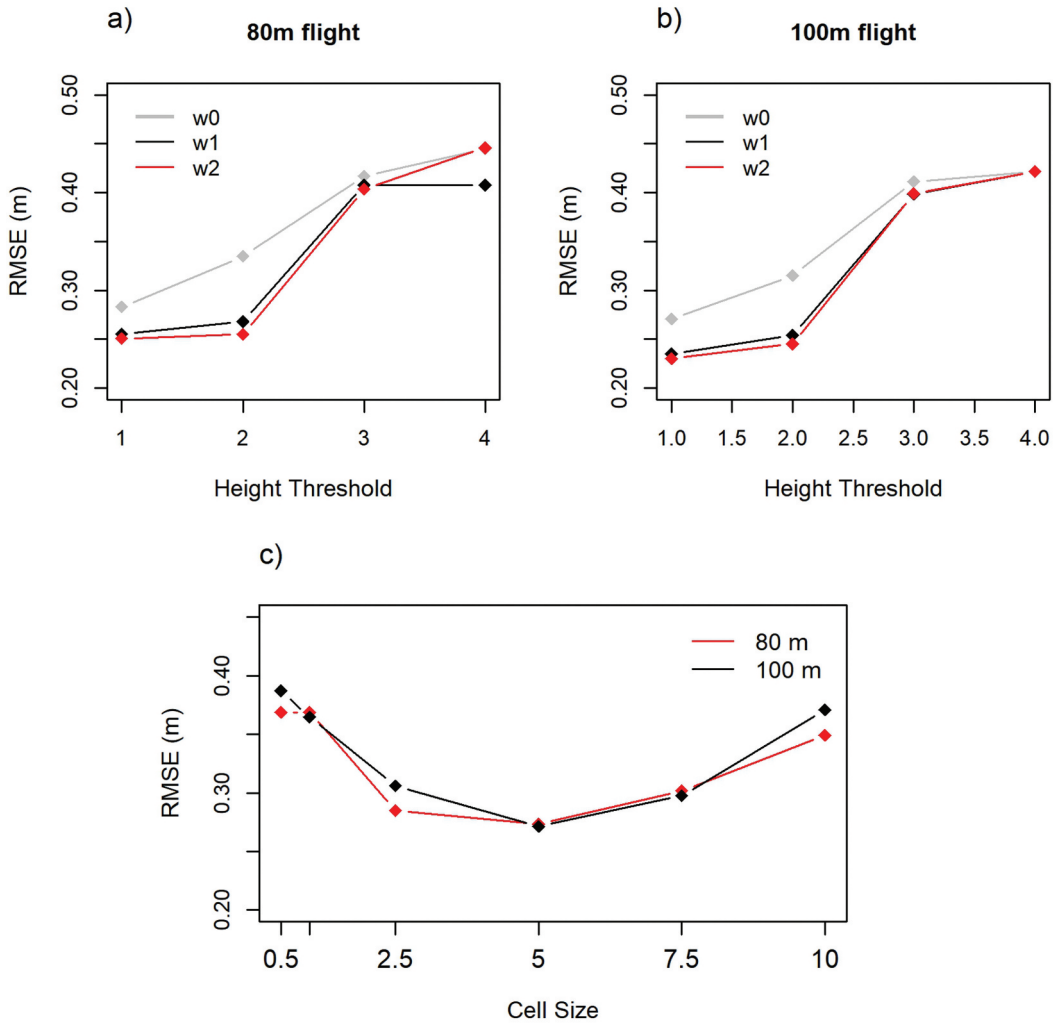

Figure 4. RMSE of the DTMs generated with a) PMF and a fight altitude of 80 m, b) PMF and a flight altitude of 100 m; both for window sizes of w0, w1 and w2 corresponding to intervals of 1, 2 and 3 m respectively and the height thresholds 1, 2, 3 and 4 (i.e. In ranges of 0.1–0.5, 0.1–1.5, 1.5–0.1 and 2.5–1.5,Table 2; and c) *GroundFilter* algorithm in FUSION.

[3]For more detailed statistical results of the test performed, see Appendix B2. Table B2.1 and B2.2

1.5 m) for both w2 and w1 and flight height (Table 2). In addition, for this algorithm, the ranges included in height thresholds 3 and 4, for which height iterations start from a higher to lower value, yielded higher RMSE values than the iterations that start from a lower value and end at a higher value. In the case of the parameters tested in the FUSION algorithm, the largest errors were associated with the extreme cell sizes (0.5 and 10 m) and the smallest error with the 5 m cell size. The same pattern is observed in the behaviour of NMAD, although with lower values than those obtained for RMSE (Table 4). In addition, negative values from skew, kurtosis and AMB indicate the left-skewness, greater flattening of the data than normal distribution, and the underestimation of what is predicted by LiDAR.

Although in both algorithms the best result was obtained at higher flight altitude (100 m), no relationship could be established between the parameters used for its calculation and the flight altitude, as a clear pattern of error behaviour could not be found regarding the flight height (Figure 4).

Regarding the returns obtained, in general around 50% of all returns generated by the LiDAR sensor were classified as ground by the *GroundFilter* algorithm, while the respective value was around 20% for the PMF algorithm (Table 5). However, this difference was not reflected in equal magnitude in the RMSE. In fact, less than 2 and 4 cm of difference in RMSE were found between the best results of PMF and *GroundFilter* for flight altitudes of 100 and 80 m, respectively (Table 4). This may indicate that although the PMF locates a smaller number of ground returns, these will be sufficiently representative for effective interpolation of a valid DTM. In addition, in all cases, more than 97% of the points classified as ground corresponded to the first return.

On the basis of the above, the ground classification used in the rest of the study was that obtained with the PMF algorithm for a window size w2, height threshold of 0.1 to 0.5 m and the flight of altitude 100 m. Figure 5 shows the results of the comparison of elevations (Z) calculated with UAV LiDAR and GNSS-RTK field data. In part (a) of this graph, it can be observed that all the points are located above the 1:1 line (), which indicates underestimation of the Z dimension.

CHM and Shrub height

The best fit between model and reference for the vegetation height was obtained at a resolution of 0.25 m for the CHM and is shown in Figure 6. The distribution of the observed heights is plotted in graph a) with outliers of heights less than 0.5 m and greater than 2.5 m. As observed in part b) most of the sampling points are located above the 1:1 line, which indicates a general tendency for overestimation of the heights. There are also 8 points with observed heights of less than 0.5 m and that a priori do not correspond to the shrub vegetation under study. In c) the elimination of points of height less than 0.5 m (and therefore not corresponding with scrub

Table 5. Distribution of returns in the ground filtering.

				Percentage (%)	
Algorithm	Flight altitude	Nº of ground returns	Density of ground returns (returns/m^2)	Ground returns	1st Return
PMF	80 m	2753354	72,48	17%	97%
	100 m	2795849	73,41	14%	98%
FUSION	80 m	8303130	212,25	51%	98%
	100 m	10625882	270,30	51%	99%

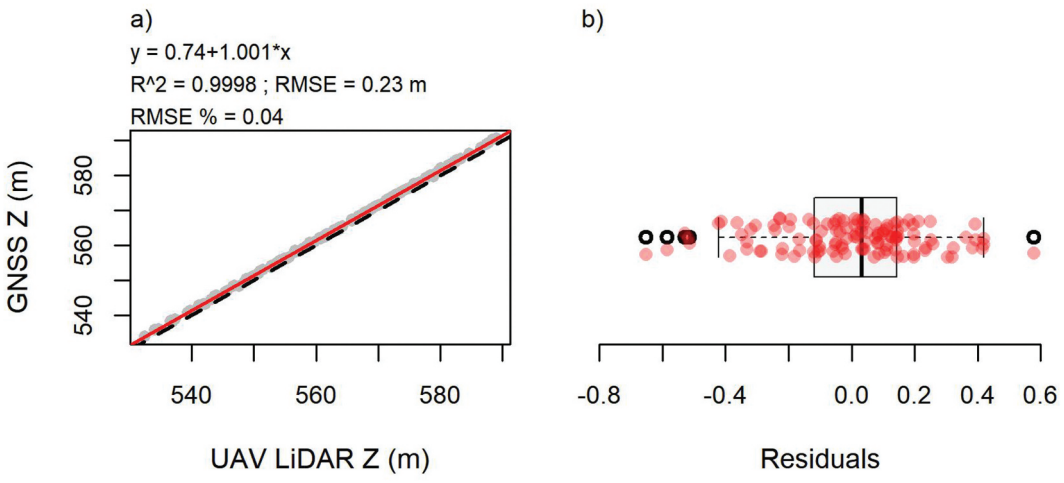

Figure 5. a) simple linear regression for DTM - PMF, window size w2 and threshold 1 during a 100 m flight and b) residuals.

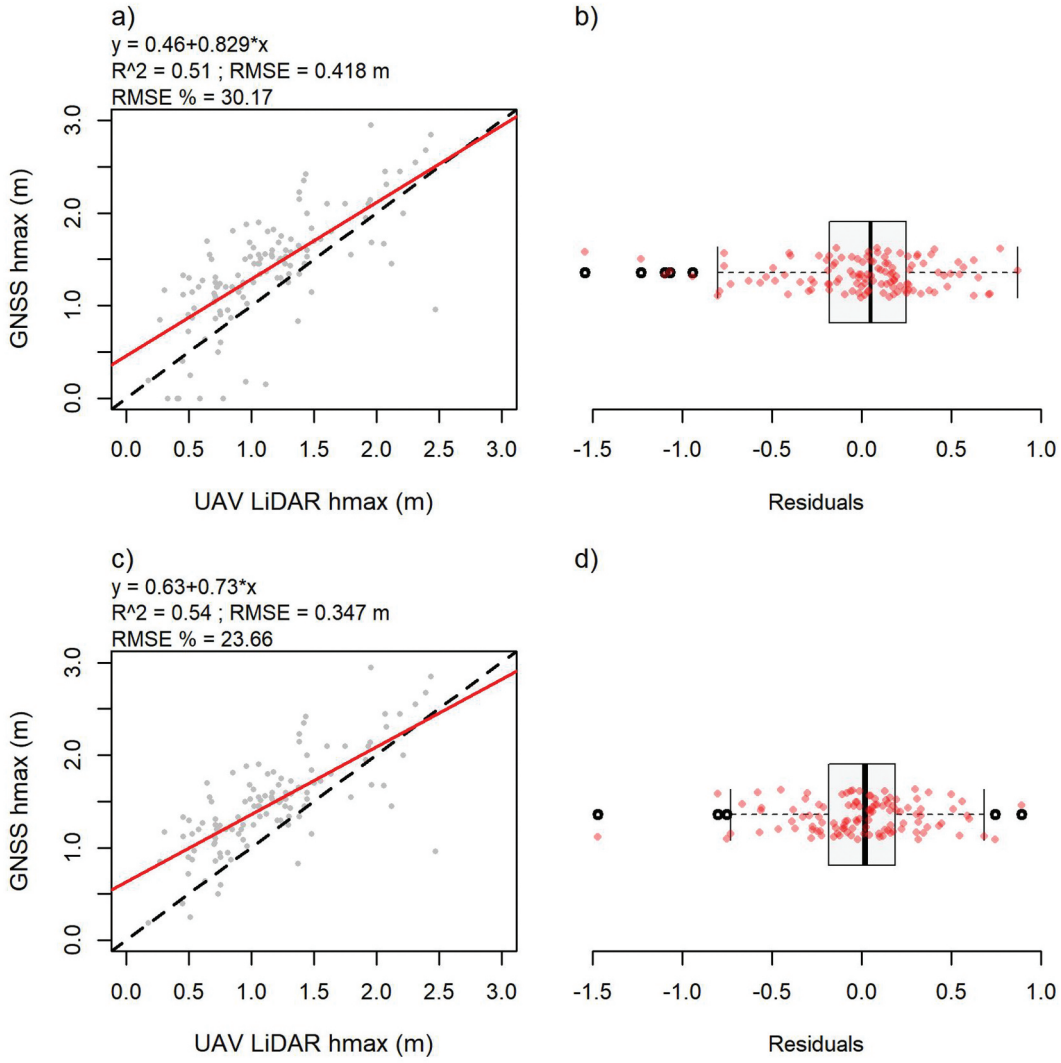

Figure 6. Linear regression and residuals for PMF, window size w2 and threshold 1 during a 100 m flight: a), b) CHM, including outliers of heights < 0.20 m and c), d) CHM after removal the outliers of heights < 0.20 m.

vegetation) improved the fit and greatly reduced the RMSE. Additionally, the observed bias was −0.27.

On the other hand, in the visualizations of the DTMs and CHMs generated by the best result from each algorithm assessed in this study, as shown in Figure 7 (PMF) and Figure 8 (*GroundFilter*), the rough texture observed in the DTM (bottom right-hand corners) may indicate that the ground filtering is apparently classifying vegetation returns as ground returns leading to an irregular ground pattern.

Effect of shrub cover characteristics and vegetation height on height estimation

The values of the Absolute Error (AE) and the Relative Error as a percentage (PE) for the different classes of shrub cover (in accordance with the categories established in Table 3) are shown in Figure 9. Although visually it appears that the AE and PE could be different for the low-density gorse (LD) cover and the other categories, ANOVA analysis of the data showed that there are no significant differences between the error distribution of the categories of vegetation cover examined (Table 6).

Regarding the influence of the different heights of the shrub, in Figure 10 we can observe in a) larger errors in the categories comprised between 1 and 2 m although with slight variations in the intermediate values and in b) a decrease in the relative error for the taller height classes, of 56.99% for the range 0.5 to 1 m to 20.43% for the higher above 2.5 m. In accordance with the ANOVA results (Table 7) the null hypothesis was accepted for the AE and rejected it for the RE, thus confirming the existence of possible significant differences in the RE depending on vegetation height.

According to the equivalence test, the effect of coverage and height categories in absolute error is equal to zero. This conclusion is also supported by the partial eta-squared (η_p^2) for equivalence presented in Tables 6 and 7, showing a higher proportion of total variance explained by the factor in PE.

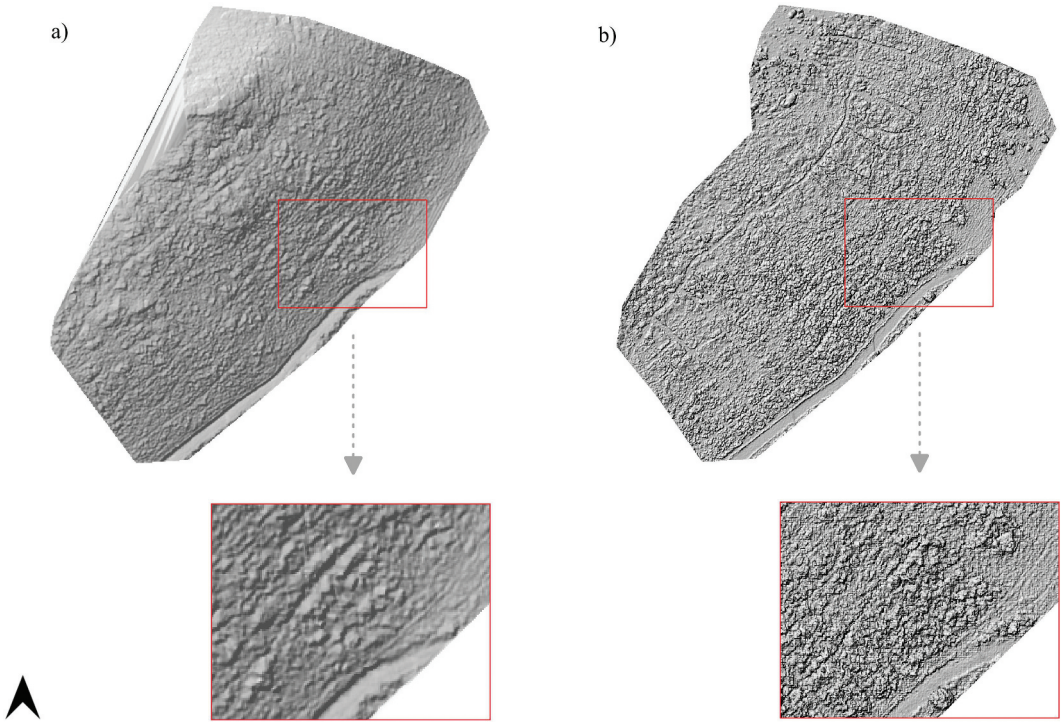

Figure 7. Graphical representation of the results obtained with the PMF algorithm: a) DTM obtained with a window size of 3 m (w2) and height threshold range of 0.1 to 0.5 m and b) CHM at a resolution of 0.25 m. The rough, irregular texture of the ground surface can be observed in detailed view of the CHM.

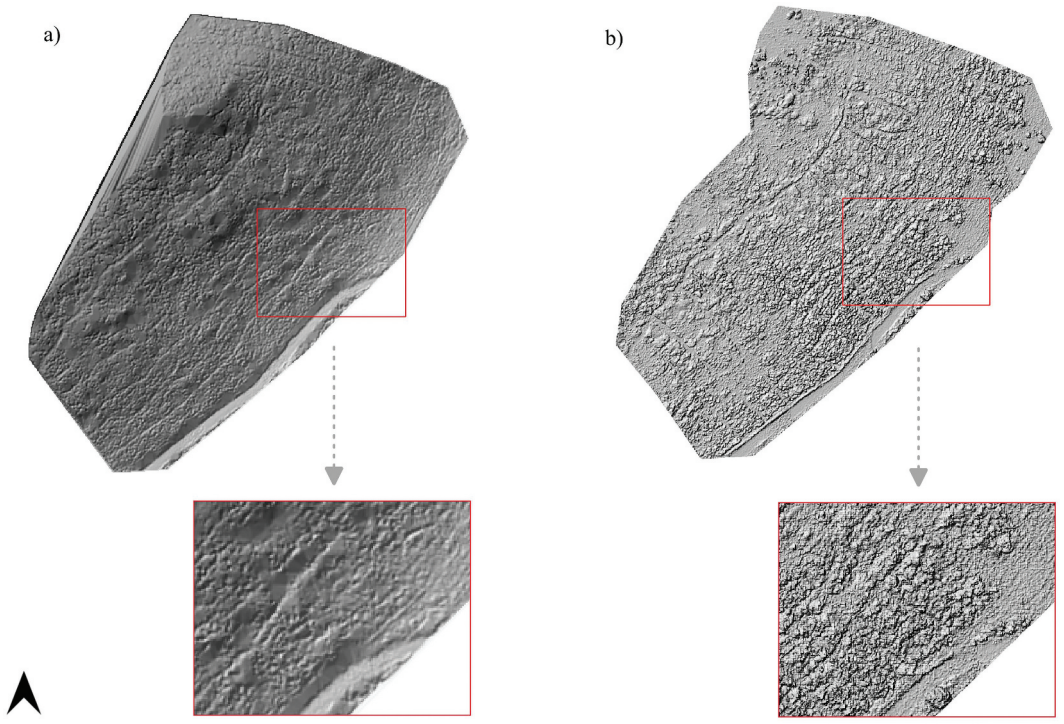

Figure 8. Graphical representation of the results obtained with the ground filter FUSION algorithm: a) DTM obtained for a cell size of 5 m and b) CHM at a resolution of 0.25 m. The rough, irregular texture of the ground surface can be observed in detailed view of the CHM.

Effect of reducing the density of the point cloud on estimation of shrub height and DTM accuracy

The RMSE values in the DTM estimation varied as a result of the reduction in the density of points in the original point cloud, while R^2 coefficient remained almost constant at all densities tested and for both flights (Figure 11). For the flight of altitude 80 m, the RMSE value scarcely varied up to a reduced density of 50 points/m^2, after which the RMSE value increased gradually to 7.4 cm for a density of 1 point/m^2.

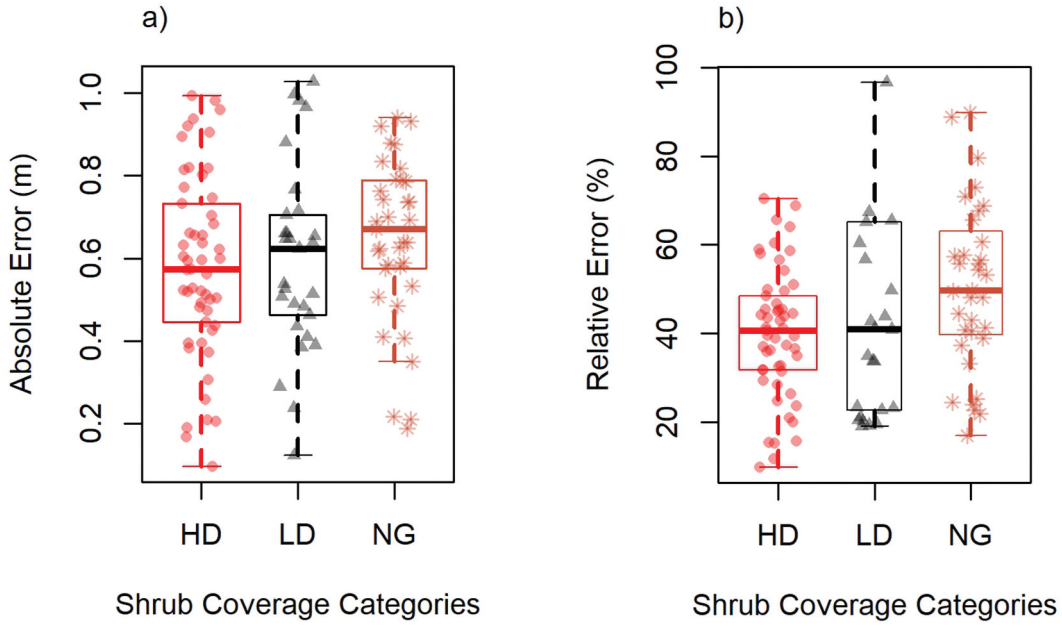

Figure 9. Variation in the gorse cover categories in the study area a) absolute error and b) relative error. The box plot shows the mean error for each category. The difference in the width of the boxes indicates the sample size in each category. The categories on the X axis correspond to very dense gorse (HD), low density of gorse (LD) and no gorse (NG). Heights below 0.5 m are not included.

Table 6. F ANOVA statistic, associated probability and partial eta-squared (ηp^2) for the equivalence test (at α: 0.05 significance level) (cover).

	F	*p-value*	η_p^2		F	*p-value*	η_p^2
AE	1.312	0.2733	0.08	PE	3.991	0.021*	0.15

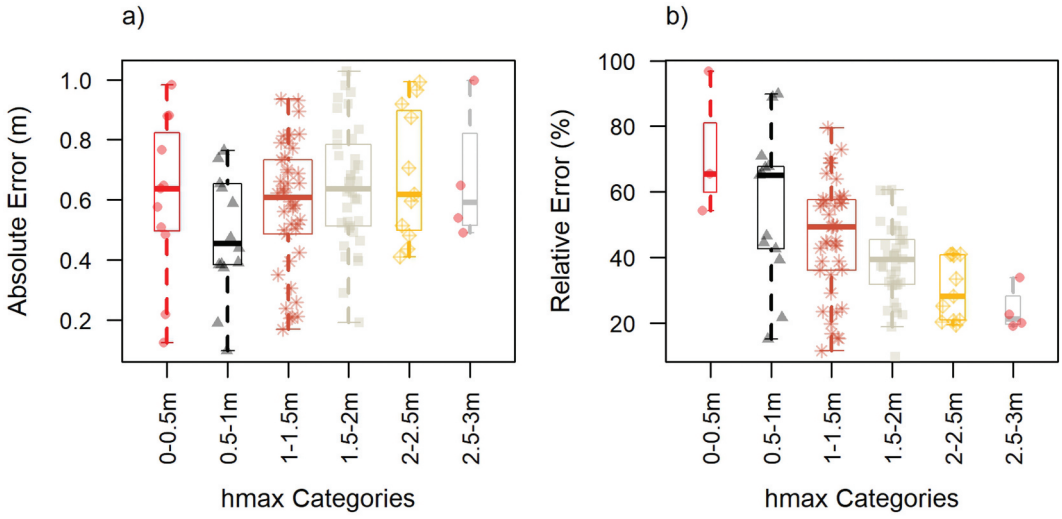

Figure 10. Variation between the height categories in the (a) absolute error and (b) the relative error. The boxplots show the mean error for each category. The difference in width represents the size of sample in each category. Heights of less than 0.5 m are not included.

Table 7. F ANOVA statistic, associated probability and partial eta-squared (ηp^2) for the equivalence test (at α: 0.05 significance level) (height).

	F	p-value	η_p^2		F	p-value	η_p^2
AE	2.117	0.1483	0.09	PE	20.165	<0.001	0.37

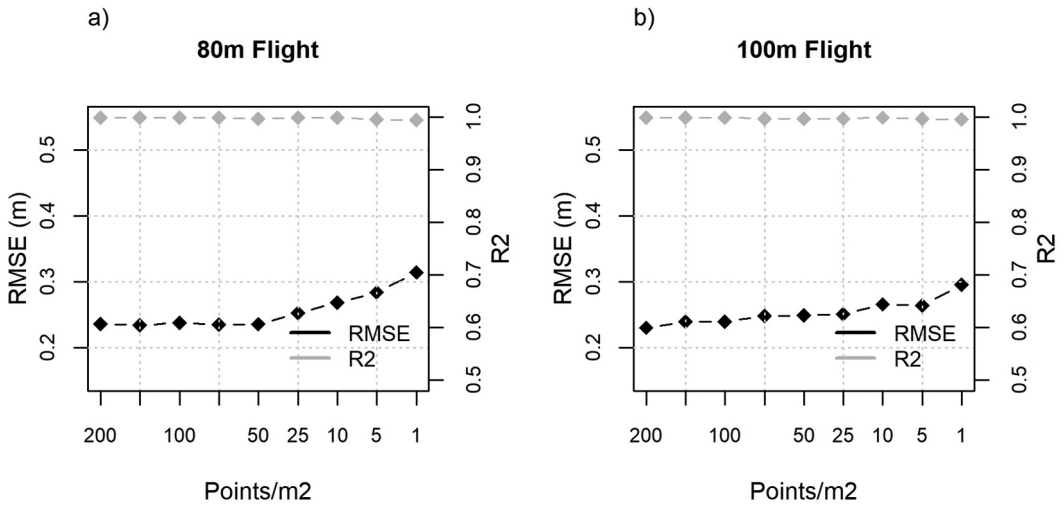

Figure 11. Analysis of the effect of the reduction in point cloud density on the accuracy of the DTM for a window size of w2, intervals of 3 m and a height threshold range of 0.1 to 0.5 m for a) a flight altitude of 80 m and b) a flight altitude of 100 m.

Conversely, for the flight of altitude 100 m the RMSE remained constant up to a density of 100 points/m^2, varying slightly (by 1 cm) between this density and a density of 25 points/m^2. In this case, the total increase in the error when the resolution of the original point cloud decreased to 1 point/m2 was 6.5 cm.

Likewise, the effect of the reduction in point density on the accuracy of the CHM followed a similar pattern to that observed for the elevations, although in this case the value of the R^2 coefficient decreases and does not remain constant at all densities tested (Figure 12). For the flight of altitude 80 m (Figure 12a), the RMSE value remained relatively constant (0.34 m) up to a density of 50 points/m^2, although it was slightly higher (by 0.5 cm) than for a density of 100 points/m^2. The greatest loss of accuracy was produced at densities lower than 25 points/m^2 with a 1.5 cm increase in the error. This was also observed in the R^2 values, although the decrease in accuracy was greatest at densities higher than 50 points/m^2. The same was observed for the flight altitude of 100 m (Figure 12b), although the effect was less pronounced and the RMSE can be considered to have remained constant up to a density of 25 points/m^2. The increases in error between the original density and a density of 1 point/m^2 were 4.3 and 3.9 cm for the flight altitudes of 80 and 100 m, respectively.

All of the findings reported above indicate that a reduction in density to 50 points/m2 apparently does not lead to variations in R^2 and RMSE and that in some cases a density of 25 points/m^2 will not greatly affect the RMSE. Thus, the minimum range of density of ground returns required to obtain acceptable estimates, without important loss of accuracy, can be established at between 7 and 13 points/m^2. Refer to Table 8 for detailed density information from the study flights.

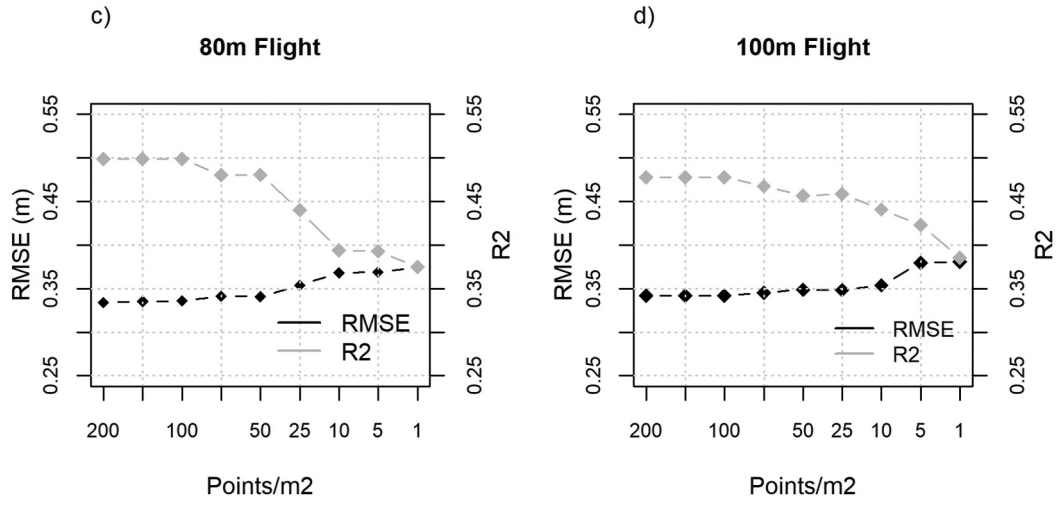

Figure 12. Analysis of the reduction in point cloud density in the vegetation height estimation accuracy for a window size w2, intervals of 3 meters and height threshold range 0.1 to 0.5 m for c) a flight altitude of 80 m y d) a flight altitude of 100 m.

Table 8. Distribution of the density of ground returns after density reduction.

Density reduction up to (points/m^2)	Flight of 80 m (Ground points/m^2)	Flight of 100 m (Ground points/m^2)
200	45.66	39.46
150	35.20	30.85
100	24.59	29.80
75	19.02	17.23
50	**13,32**	12,20
25	**7,26**	**6,82**
10	3,33	3,17
5	1.84	1.79
1	0.41	0.41

Discussion

Shrub height and DTM

In this study, we propose and validate with non-destructive techniques a method based on UAV LiDAR systems to estimate vegetation height in steeply sloping areas of dense shrub. A moderate correlation ($R^2 = 0.51–0.54$) between the observed and estimated values was detected, and the accuracy measured by RMSE was 0.34 m in the best cases. Moreover, scatter plots of the estimated versus observed heights revealed a general tendency for heights above 0.2–0.5 m to be underestimated (Figure 6a). Below this threshold, the variability in the estimated height was greater and the laser tended to overestimate the values with a skew of up to 1.20 m, indicating a low level of reliability in this range.

Comparison of the R^2 and RMSE values obtained in the present study between the observed and estimated by LiDAR height of the vegetation with those obtained in previous studies carried out in different vegetation scenarios shows that our values fall between the best (Hartley et al., 2020; Miura et al., 2018; Watt et al., 2014) and worst (Zhao et al., 2022) results (see Appendix A1, Table A1 for a more thorough review of the state of the art on the topic). However, the highest levels of accuracy and strongest correlations in the literature were obtained with a superior quality DTM generated with data collected under optimal conditions that guaranteed sufficiently high numbers of ground returns (open vegetation canopy, flights conducted after fire or sowing, etc.).

The relationship between a good quality DTM and the reliability of estimation of forest metrics is well documented (Estornell, Ruiz, et al., 2011b, 2011a; Riaño et al., 2007; Watt et al., 2014). In processing LiDAR data for this purpose, point cloud classification is crucial. In view of this, two ground filtering algorithms were tested and evaluated, with the PMF algorithm performing best for this task, although there was a minor difference in the reliability of the estimates obtained (≈4 cm). In addition, PMG-processed estimates became more accurate as the window size increased (from 1 to 3 m). These findings are consistent with those observed in (Estornell, Ruiz, et al., 2011a), in which in very steep slopes, including the areas of *Quercus coccifera* shrub, the lowest RMSE value (0.24 m) corresponded to window sizes of 2 and 3 m. However, in contrast to the findings of the present study, the highest RMSE values occurred at the lowest threshold interactions. This discrepancy may arise due to technical modifications in the PMF algorithm implementation on *lidR*. While the original method relies on raster data, *lidR* employs point-based morphological operations, and this could explain because the PMF filter classifies almost all points as ground points of height threshold of 3 and 4 (cf. Appendix B1, Table B1).

Despite the tests conducted, some roughness on the land surface was observed in the DTMs generated, which may indicate that the algorithms used classified points corresponding to vegetation as ground points. The poor performance of ground filtering algorithms in dense low-lying vegetation and the consequent loss of reliability of the data have been reported in previous studies (Curcio et al., 2022; Riaño et al., 2007; Zhao et al., 2022). The performance of the algorithm is restricted by the scant difference between the height of the ground and the maximum height of the shrub vegetation, as well as the irregularities in the vegetation cover and the ground surface, such as the presence of rocks and layers of dead biomass. Such irregularities reduce the capacity of the pulse to penetrate the vegetation and lead to greater dispersion of the returns from the lower layers of the stratum. Accordingly, multispectral data are often included in order to increase the accuracy of classification and thus overcome the restriction caused by the dispersion of LiDAR points, although this solution increases the complexity and cost of data acquisition. Previous studies have reported that for sloping shrub areas the inclusion of multispectral data increased the R^2 from 0.48 to 0.65 (Riaño et al., 2007) and in saltmarsh zones, it decreased the RMSE from 0.11 to 0.06 m (Curcio et al., 2022) and from 0.65 to 0.40 m (Medeiros et al., 2015).

Nevertheless, and as observed in other recent ULS-based studies, validation using the relationship between the elevations of the field sampling points and those estimated by ULS yielded a stronger correlation ($R^2$0.9998), although the error was slightly higher than that obtained in these studies (RMSE = 0.23 m). For instance, in salt marshes with *Sarcocornia* cover, scanned using the same LiDAR sensor as in the present study, the R^2 value exceeded 0.86, with a RMSE below 0,14 m (Curcio et al., 2022), and in meadow steppe, the respective values were 1 and 0.10 m (Zhao et al., 2022). The higher RMSE values obtained in the present study can be attributed to: (i) the more complex vegetation type in the present study, including heterogeneous structure and a layer of dead organic matter (≈7 cm of thickness in 70% of the point

sampled); (ii) the possible effect of the slope, as previous studies were conducted in relatively flat areas; and/or (iii) potential problems derived from the lower accuracy of the ground point filtering. This finding is supported in the present case by the analysis of the distribution of the LiDAR returns, where over 97% of the returns corresponded to first returns, rendering second and third returns symbolic.

The high correlations obtained during DTM validation contrast with the estimates of vegetation heights from CHM. Specifically, the CHM exhibited nearly half the correlation and a RMSE approximately 11 cm greater than for the DTM. The same pattern was observed in (Curcio et al., 2022) and (Zhao et al., 2022) with R^2 below 0.105 and RMSE ranging from 0.123 to 0.183 m (for a pixel size of 0.02 m) and R^2 = 0,17 and RMSE = 0,40 m obtained for the CHM, respectively, compared to the DTM values mentioned earlier. In this respect, the higher RMSE value obtained in this study (0.23 m) may be associated with the following: (i) the complexity of the surface analysed; (ii) the greater difficulty associated with field measurements; (iii) the spatial resolution of the LiDAR height measurements (0.25 m) relative to that of the sampling (0.10 m); and/or (iv) the ground point filtering (Wieser et al., 2016).

Additionally, the observed tendency for underestimation of LiDAR-derived vegetation heights has been widely across various forest scenarios (Dandois et al., 2015; Wieser et al., 2016; Miura et al., 2018; Streutker & Glenn, 2006; Riaño et al., 2007; Zhao et al., 2022; Curcio et al., 2022; X. Zhang et al., 2021). Another possible cause, apart from those mentioned in the previous paragraph, is that the frequency of the laser scanner is insufficient for the speed at which the flight is executed with the UAV, which would lead to a loss of information corresponding to the upper part of the vegetation (Curcio et al., 2022; X. Zhang et al., 2021; Ma et al., 2017). In this manner, a recent study conducted in meadow steppe showed that the loss of information is more common in the upper part of the vegetation than in the lower part, and that the loss is mainly influenced by the maximum height of the vegetation, its standard deviation, and the flight altitude (Zhao et al., 2022). The greatest influence of this effect for the maximum height is attributed to the fact that in shrublands, mostly relatively continuous, its measurement could be assimilated to sharp structures with the consequent lower likelihood of a correct estimation (Roussel et al., 2017; Zhao et al., 2022). In this respect, the inventory method used in this study, focusing on maximum height at a single point (apical shoot of a shrub), may be subject to this effect rather than measuring the maximum point average in a determined area.

In the same way as for the underestimation, the above may also explain the lower correlation obtained for the CHM than for the DTM (Curcio et al., 2022; Zhao et al., 2022). However, as the flight speed was 7 m/s in the present study, the causes are more likely to be related to erroneous reading of the height due to the spatial resolution or the limitations of the equipment used in this type of area. Nonetheless, future studies should focus on analysing the loss of information regarding the vegetation cover measured by LiDAR sensors.

Furthermore, the lower reliability of height estimates in scrubland formations lower than 0.5 m is consistent with previously reported findings (Hartley et al., 2020; Riaño et al., 2007; Su & Bork, 2006). In this context, the difficulties that LiDAR has in reaching the ground in areas of dense low-lying vegetation lead to systematic errors of up to 0.15 m (Alizad et al., 2020; Chassereau et al., 2011; Curcio et al., 2022). The largest systematic error found in this study (−0.27 m) could be related to the layer of dead biomass. Additionally, this error may also be intensified by the sources of error previously discussed (the complexity of vegetation, spatial resolution, etc.).

Finally, the estimates obtained by the 100 m flight were slightly more accurate than those obtained by the 80 m flight. This finding is consistent with previously reported observations for flight altitudes of 100 and 60 m and the same LiDAR sensor (RMSE = 0.115 and 0.089 respectively) (Curcio et al., 2022). Although the above may indicate a decrease in the flight altitude does not improve the results significantly, it has previously been noted that the height of the vegetation canopy will remain constant in relation to the flight altitude, but with large variations in the standard deviation (X. Zhang et al., 2021). This leads to suggesting the need to conduct studies at lower flight altitudes (e.g. at 40 m AGL) to evaluate their performance. In this respect, greater loss of information in LiDAR data on maximum vegetation heights has been associated with high flight altitudes (Zhao et al., 2022). Moreover, in another study, different pulse frequencies and a flight altitude of 20 m yielded the same point density as a flight of altitude 40 m, indicating that there may be a threshold altitude above which no improvement in results is obtained (Bouziani et al., 2021).

The flights executed in the present study differed both in altitude and in the lateral overlap, which was higher in the 100 m flight. The most obvious consequence of this difference was an increase in the point density, although this was not reflected in a greater accuracy of the LiDAR-derived estimates. In addition, there was no increase in the number of second and third returns, which may have been expected as the overlaps coincided with off-nadir angles. It appears that greater overlap may lead to an increase in the error associated with the point cloud and thus eliminate the benefits associated with the additional cover, and it is therefore not recommended (Bouziani et al., 2021; Hartley et al., 2020; Liang et al., 2019).

Influence of the shrub cover characteristics and vegetation height

Diverse studies have confirmed the effect that the vegetation type has on the accuracy of the DTM and therefore on the LiDAR-derived estimates of the metrics (Watt et al., 2014). Thus, in one such ALS-based study, the RMSE values were in the range 0.10 to 0.59 m (mean, of 0.47 m), and the type of vegetation was found to be the most important factor affecting the accuracy of the DTM (Su & Bork, 2006). In another study, the RMSE values were in the range 0.25 to 0.41 m, and the highest values were associated with areas of dense shrub (Estornell, Ruiz, et al., 2011a). In a ULS-based study, the highest RMSE value (0.128 m) corresponded to areas of *Sarcocornia* sp. cover in saltmarshes (Curcio et al., 2022).

Interestingly, no significant differences were observed in relation to the category of vegetation cover and/or the density of vegetation in the present study, and the absolute errors and relative errors were similar for compact gorse formations, isolated shrubs and ferns and herbaceous vegetation. This finding contrasts with those reported in the above-mentioned studies conducted in different scenarios. The lack of difference observed in the present study may be attributable to the fact that the data acquisition flights were conducted during a period of maximum plant growth (Su & Bork, 2006), when almost all of the surface was covered by dense green vegetation, sometimes mixed with woody remains. For example, the fern cover was at its peak of height and coverage at the survey time, whereas a winter or early spring flight could have shown more clear differences. A more detailed analysis of this aspect is required.

Regarding the errors related to the distribution of the shrub heights, there were no significant differences between the categories in terms of the absolute error, although there were significant differences in terms of the relative error. This may be a consequence of the formulas used to calculate the errors. Additionally, for ULS, errors followed a similar pattern, albeit with higher values than those observed in a study of isolated trees (Hartley et al., 2020). In that study, absolute errors showed no significant differences with tree height, except for trees shorter than 1 m, while relative errors decreased as tree height increased.

Our findings confirm that the methodology might be effective under scrub types characterized by a high degree of complexity. In fact, one of the premises of this work was to test the potential of ULS for the characterization and monitoring of key issues as the coverage and height of scrubs in relation to habitat management and conservation. In this regard, an accurate description of 3D vegetation structure might support the identification of conservation problems related to habitat encroachment and in its case support decision-making on grazing pressures and even on the design and monitoring of conservation measures.

Effect of reducing the density of the point cloud

The study findings confirm that reducing the density of the original point cloud to between 25 and 50 points/m^2 — resulting in ground returns between 7 and 13 points/m^2 — does not imply loss of accuracy of more than 1 cm in the DTM or vegetation height estimates for the considered flight altitudes.

As far as we are aware, no previous studies have addressed this factor in relation to ULS; however, the above-mentioned findings are consistent with those obtained in previous studies for ALS. Thus, in a study considering the effect of density point reduction on the DEM accuracy, covering an area of 6.900 km^2 in Australia, including shrub growing on gentle slopes, the authors concluded that the variations in RMSE began to be observed for density reduction less than 50% on an initial spacing of around 2.4 m, although the increase was particularly marked after a 75% reduction (Liu & Zhang, 2008). Likewise, in a study conducted in a steeply sloping area including dense shrub in Valencia (East of Spain), changes in the RMSE began to be observed for point densities lower than 8 points/m^2, for a DTM obtained with the same classification algorithm and window size as used in the present study (Estornell, Ruiz, et al., 2011a). Moreover, the increase in error associated with reducing the original density to 1 point/m^2 was between 6 and 11 cm, which is similar to the increase observed in the present study (6.5–7.5 cm, depending on the flight altitude). Similar results were obtained for young Douglas fir plantations in New Zealand, and a good quality DTM guaranteed with a minimum of 10 points/m^2; the reduction in point density to 1 point/m^2 allowed estimation of the canopy height with the benefit of reducing the amount of redundant data and increasing the efficiency in terms of data storage and processing time (Watt et al., 2014).

Nonetheless, the study findings should be considered with caution. The study area is characterised by very dense vegetation cover of heterogeneous structure, and the slope, although steep, is homogeneous. Hence, reduction in the point density for other reasons should be carried out so that the critical elements and identifiers of characteristic land elements are retained and that only less important elements are eliminated (Chou et al., 1999; Liu & Zhang, 2011).

Conclusions

The present study evaluated the applicability of using light UAVs (specifically the DJI Zenmuse L1) in areas of complex vegetation. The findings indicate

that the vegetation cover was able to be penetrated, even in dense areas of shrub, although some restrictions were noted. In this case, penetration of the vegetation cover was mainly influenced by the presence of a layer of dead biomass, not discounted from the total observed measurement of about 7 cm thickness through which the LiDAR pulse cannot penetrate. The performance of the sensor and/or deficiencies in ground point filtering are also important factors affecting penetration of the vegetation. Thus, various authors have suggested complementing the information derived from LiDAR sensors with spectral data and/or have investigated and generated other ground classification algorithms. However, the lower correlation obtained for vegetation height ($R^2 = 0.51–0.54$) than for elevation (R^2 0.9998), consistent with previous findings, suggests that this may not only depend on problems associated with penetration of vegetation cover or ground filtering but also on the reliability of height validation measurements, e.g. the difference in the sample size for observed and estimated data and the possible loss of information in the upper layer of vegetation derived from LiDAR data. In this context, analysis of the different flight altitudes revealed that this factor may have a greater influence on the accuracy of the results obtained with the sensor used than the greater density of points originated by the increase in the lateral overlap during the flight.

On the other hand, no differences in height estimation errors were observed based on gorse density (very dense, dense, or absent) or when estimating different shrub cover heights. This finding, which contrasts with those of previous studies, may be attributed to the inclusion of tall plants with some woody fractions within vegetation categories, even in herbaceous-dominated classes, and due to the dense coverage of green vegetation.

For the implications regarding improvement of the data handling, storage and processing time, special mention must be given to the possible reduction in the density of the original point cloud up to 25–50 points/m^2 without loss of reliability of the data obtained with the LiDAR sensor.

In general terms, the findings indicate that in areas of dense low-lying vegetation, ULS flights should be conducted during periods of low vegetative growth, particularly of herbaceous vegetation and ferns, and with higher pulse frequencies, lower flight altitude, lower lateral overlap, and low speed to guarantee less loss of information required for estimation of CHMs. In addition, larger sample sizes may provide better results for the maximum height variable. However, further investigation is required in order to define the optimal flight parameters for ULS and to evaluate the loss of information from the upper layer of the shrub canopy.

Despite the well-known limitation of lightweight UAV sensing due to their relatively low yield on wide areas in comparison to satellite or conventional airborne systems, this work shows the potential of ULS in conservation problems related to the vegetation 3D structure. It allows the detection of pattern–process relationships at a sub-metric scale, which coarser resolutions would neglect, and it might be extrapolated to other scenarios of fine-scale habitats relying on a delicate climate and management balance.

Acknowledgments

This work was carried out as part of the project Predoctoral Researcher in Training, included in professional group I.2, to carry out research functions in "Realization of this research project linked to the research line of the project "Characterization and monitoring of biodiversity through multiscale analysis of remote sensing data "UAS satellite", in relation to the Campus Terra Agreement: Strengthen the research career, in accordance with the professional classification system in force in the company, in Department of Botany, Escola Politécnica Superior de Enxeñaría, Campus de Lugo, USC

Disclosure statement

No potential conflict of interest was reported by the author(s).

Funding

This work was supported by the Xunta de Galicia (Consellería de Cultura, Educación, Formación Profesional e Universidades) under Grant Research Competitive Reference Group (GRC GI-1809 BIOAPLIC, ED431C 2019/07); Universidade de Santiago de Compostela, Campus Terra, GI-1809 under Grant "Contrato 2022-AD013 ao abeiro do Convenio de Colaboración entre a USC e a Consellería de Cultura, Educación e Universidades polo que se regula o Campus de Especialización Campus Terra"; flights were supported by LIFE Nature and Biodiversity Programme, European Union under Grant Life in Common Land (LIFE16 NAT/ES/000707).

ORCID

P. Rodríguez Dorribo http://orcid.org/0009-0006-2175-3927
C. Alonso Rego http://orcid.org/0000-0002-2528-0059
R. A. Díaz Varela http://orcid.org/0000-0001-6094-2153

Data availability statement

The participants of this study did not give written consent for their data to be shared publicly as the survey was done on private ownership, so due to the sensitive nature of the research supporting data is not available.

References

«*Bosques españoles y su evolución*». s. f. Accedido 18 de diciembre de 2023. https://www.miteco.gob.es/es/biodiversidad/temas/inventarios-nacionales/inventario-forestal-nacional/index.html

Acre Surveying Solutions, dir. (2021). *DJI L1. Todo lo que quieres saber del nuevo LIDAR de DJI*. https://www.youtube.com/watch?v=rsQpTMDYCys

Ahokas, E., Kaartinen, H., & Hyyppä, J. (2003). A quality assessment of airborne laser scanner data. *The International Archives of Photogrammetry, Remote Sensing & Spatial Information Sciences*, *34*(enero), 1–7.

Alizad, K., Medeiros, S. C., Foster-Martinez, M. R., & Hagen, S. C. (2020). Model sensitivity to topographic uncertainty in meso- and microtidal Marshes. *IEEE Journal of Selected Topics in Applied Earth Observations & Remote Sensing*, *13*, 807–814. https://doi.org/10.1109/JSTARS.2020.2973490

Anderson, E. S., Thompson, J. A., Crouse, D. A., & Austin, R. E. (2006). Horizontal resolution and data density effects on remotely sensed LIDAR-Based DEM. *Geoderma*, *132*(3–4), 406–415. https://doi.org/10.1016/j.geoderma.2005.06.004

Baltensweiler, A., Walthert, L., Ginzler, C., Sutter, F., Purves, R. S., & Hanewinkel, M. (2017). Terrestrial laser scanning improves digital elevation models and topsoil pH modelling in regions with complex topography and dense vegetation. *Environmental Modelling & Software*, *95*(septiembre), 13–21. https://doi.org/10.1016/j.envsoft.2017.05.009

Baltsavias, E. P. (1999a). A comparison between photogrammetry and laser Scanning. *ISPRS Journal of Photogrammetry & Remote Sensing*, *54*(2–3), 83–94. https://doi.org/10.1016/S0924-2716(99)00014-3

Baltsavias, E. P. (1999b). Airborne laser scanning: Existing systems and firms and other Resources. *ISPRS Journal of Photogrammetry & Remote Sensing*, *54*(2–3), 164–198. https://doi.org/10.1016/S0924-2716(99)00016-7

Blanco Arias, C. A., Varela, E. R. D., Barcia, C. V. M., Abarzuza, L. L., Díaz, J. F., & Varela, R. A. D. (2018). Buen estado de conservación de turberas y brezales húmedos en la ZEC Serra do Xistral. (LIFE16 NAT/ES/000707). Lugo, Spain: Deputación de Lugo, Universidade de A Coruña & Universidade de Santiago de Compostela. https://www.lifeincommonland.eu/uploads/files/190528_DelE3.1_DosierPropietarios_ESP.pdf

Bouziani, M., Amraoui, M., & Kellouch, S. (2021). Comparison assessment of digital 3d models obtained by drone-based lidar and drone imagery. *International Archives of the Photogrammetry, Remote Sensing and Spatial Information Sciences* XLVI-4-W5-2021 (diciembre): *XLVI-4/W5-2021*, 113–118. https://doi.org/10.5194/isprs-archives-XLVI-4-W5-2021-113-2021

Brede, B., Lau, A., Bartholomeus, H., & Kooistra, L. (2017). Comparing RIEGL RiCOPTER UAV LiDAR derived canopy height and DBH with terrestrial LiDAR. *Sensors (Switzerland)*, *17*(10), 2371. https://doi.org/10.3390/s17102371

Caldwell, A. R. (2022). *Exploring equivalence testing with the updated TOSTER R Package* (Preprint ed.). PsyArXiv. https://doi.org/10.31234/osf.io/ty8de

Campbell, H., & Gustafson, P. (2021). *What to make of non-inferiority and equivalence testing with a post-specified margin?*. *arXiv*. http://arxiv.org/abs/1807.03413

Chassereau, J. E., Bell, J. M., & Torres, R. (2011). A comparison of GPS and Lidar salt marsh DEMs. *Earth Surface Processes and Landforms*, *36*(13), 1770–1775. https://doi.org/10.1002/esp.2199

Chou, Y.-H., Liu, P.-S., & Dezzani, R. (1999). Terrain complexity and reduction of topographic data. *Journal of Geographical Systems*, *1*(julio), 179–198. https://doi.org/10.1007/s101090050011

Curcio, A. C., Peralta, G., Aranda, M., & Barbero, L. (2022). Evaluating the performance of high spatial resolution UAV-Photogrammetry and UAV-LiDAR for salt marshes: The Cádiz bay study Case. *Remote Sensing*, *14*(15), 3582. https://doi.org/10.3390/rs14153582

Dandois, J., Olano, M., & Ellis, E. (2015). Optimal altitude, overlap, and weather conditions for computer vision UAV estimates of forest Structure. *Remote Sensing*, *7*(10), 13895–13920. https://doi.org/10.3390/rs71013895

(2014). *DECRETO 37/2014 polo que se declaran zonas especiais de conservación os lugares de importancia comunitaria de Galicia e se aproba o Plan director da Rede Natura 2000 de Galicia*. https://www.xunta.gal/dog/Publicados/2014/20140331/AnuncioCA02-270314-0001_gl.html

Deng, L., Fu, B., Wu, Y., He, H., Sun, W., Jia, M., Deng, T., & Fan, D. (2023). Comparison of 2D and 3D vegetation species mapping in three natural scenarios using UAV-LiDAR point clouds and improved deep learning methods. *International Journal of Applied Earth Observation and Geoinformation*, *125*(diciembre), 103588. https://doi.org/10.1016/j.jag.2023.103588

Díaz-Varela, R. A., Iglesias, S. C., Castro, C. C., & Varela, E. R. D. (2018). Sub-metric analisis of vegetation structure in bog-heathland mosaics using very high resolution rpas imagery. *Ecological Indicators*, *89*(junio), 861–873. https://doi.org/10.1016/j.ecolind.2017.11.068

DJI. (2021). *Especificaciones - Zenmuse L1 - DJI Enterprise*. https://dl.djicdn.com/downloads/Zenmuse_L1/20220119UM/Zenmuse_L1%20_User%20Manual_ES_v1.2.pdf

Estornell, J., Ruiz, L. A., Velázquez-Martí, B., and Hermosilla, T. (2011a). Analysis of the factors affecting LiDAR DTM accuracy in a steep shrub Area. *International Journal of Digital Earth*, *4*(6), 521–538. https://doi.org/10.1080/17538947.2010.533201

Estornell, J., Ruiz, L., & Velázquez-Martí, B. (2011b). Study of shrub cover and height using LIDAR data in a Mediterranean Area. *Forest Science*, *57*(junio), 171–179. https://doi.org/10.1093/forestscience/57.3.171

Evans, J. S., & Hudak, A. T. (2007). A multiscale curvature algorithm for classifying discrete return LiDAR in forested Environments. *IEEE Transactions on Geoscience & Remote Sensing*, *45*(4), 1029–1038. https://doi.org/10.1109/TGRS.2006.890412

Fernández-Álvarez, M., Armesto, J., & Picos, J. (2019). LiDAR-based wildfire prevention in WUI: The automatic detection, measurement and evaluation of forest Fuels. *Forests*, *10*(2), 148. https://doi.org/10.3390/f10020148

Fernández-Guisuraga, J. M., Calvo, L., Fernandes, P. M., & Suárez-Seoane, S. (2022). Short-term recovery of the aboveground carbon stock in Iberian shrublands at the extremes of an environmental gradient and as a function of burn Severity. *Forests*, *13*(2), 145. https://doi.org/10.3390/f13020145

Fraser, R. H., Olthof, I., Lantz, T. C., & Schmitt, C. (2016). UAV photogrammetry for mapping vegetation in the low-Arctic. *Arctic Science*, *2*(3), 79–102. https://doi.org/10.1139/as-2016-0008

Fu, B., Jiang, L., Yao, H., Wei, Y., Jia, M., Sun, W., Yang, Y., & Deng, T. (2024a). Retrieval performance of mangrove tree heights using multiple machine learning regression

models and UAV-LiDAR point clouds. *International Journal of Digital Earth*, *17*(1), 2392851. https://doi.org/10.1080/17538947.2024.2392851

Fu, B., Zhang, S., Li, H., Yao, H., Sun, W., Jia, M., Yang, Y., He, H., & Li, Y. (2024b). Exploring the effects of different combination ratios of multi-source remote sensing images on mangrove communities classification. *International Journal of Applied Earth Observation and Geoinformation*, *134*(noviembre), 104197. https://doi.org/10.1016/j.jag.2024.104197

Guerra-Hernández, J., Díaz-Varela, R. A., Ávarez-González, J. G., & Rodríguez-González, P. M. (2021). Assessing a novel modelling approach with high resolution UAV imagery for monitoring health status in priority riparian Forests. *Forest Ecosystems*, *8*, 61. https://doi.org/10.1186/s40663-021-00342-8

Guerra-Hernández, J., González-Ferreiro, E., Monleón, V., Faias, S., Tomé, M., & Díaz-Varela, R. (2017). Use of multi-temporal UAV-Derived imagery for estimating individual tree growth in Pinus *pinea* Stands. *Forests*, *8* (8), 300. https://doi.org/10.3390/f8080300

Hartley, R. J. L., Davidson, S. J., Watt, M. S., Massam, P. D., Aguilar-Arguello, S., Melnik, K. O., Pearce, H. G., & Clifford, V. R. (2022). A mixed methods approach for fuel characterisation in gorse (Ulex Europaeus L.) scrub from high-density UAV laser scanning point clouds and semantic segmentation of UAV Imagery. *Remote Sensing*, *14*(19), 4775. https://doi.org/10.3390/rs14194775

Hartley, R. J. L., Leonardo, E. M., Massam, P., Watt, M. S., Estarija, H. J., Wright, L., Melia, N., & Pearse, G. D. (2020). An assessment of high-density UAV point clouds for the measurement of young forestry Trials. *Remote Sensing*, *12*(24), 4039. https://doi.org/10.3390/rs12244039

Höhle, J., & Höhle, M. (2009). Accuracy assessment of digital elevation models by means of robust statistical methods. *ISPRS Journal of Photogrammetry & Remote Sensing*, *64*(4), 398–406. https://doi.org/10.1016/j.isprsjprs.2009.02.003

Hopkinson, C. (2007). The influence of flying altitude, beam divergence, and pulse repetition frequency on laser pulse return intensity and canopy distribution. *Can J Remote Sensing*, *33*(agosto), 312–324. https://doi.org/10.5589/m07-029

Hyyppä, H., Yu, X., Hyyppä, J., Kaartinen, H., Kaasalainen, S., Honkavaara, E., & Rönnholm, P. (2005). Factors affecting the quality of dtm generation in forested areas. Workshop "Laser scanning 2005" September 12-14, 2005. Working Group III/3 Enschede, the Netherlands International Society for Photogrammetry and Remote Sensing (ISPRS) (International Society for Photogrammetry and Remote Sensing (ISPRS), 85_90.

Jaakkola, A., Hyyppä, J., Yu, X., Kukko, A., Kaartinen, H., Liang, X., Hyyppä, H., & Wang, Y. (2017). Autonomous collection of forest field reference-the outlook and a first step with UAV laser Scanning. *Remote Sensing*, *9*(8), 785. https://doi.org/10.3390/rs9080785

Kaartinen, H., Hyyppä, J., Yu, X., Vastaranta, M., Hyyppä, H., Kukko, A., Holopainen, M., Heipke, C., Hirschmugl, M., Morsdorf, F., Næsset, E., Pitkänen, J., Popescu, S., Solberg, S., Wolf, B. M., & Wu, J.-C. (2012). An international comparison of individual tree detection and extraction using airborne laser Scanning. *Remote Sensing*, *4*(4), 950–974. https://doi.org/10.3390/rs4040950

Kellner, J. R., Armston, J., Markus Birrer, K. C. C., Duncanson, L., Falleger, C., Eck, C., Falleger, C., Imbach, B., Král, K., Krůček, M., Trochta, J., Vrška, T., & Zgraggen, C. (2019). New opportunities for forest remote sensing through ultra-high-density drone Lidar. *Surveys in Geophysics*, *40*(4), 959–977. https://doi.org/10.1007/s10712-019-09529-9

Klouček, T., Klápště, P., Marešová, J., & Komárek, J. (2022). UAV-Borne imagery can supplement airborne lidar in the precise description of dynamically changing shrubland woody Vegetation. *Remote Sensing*, *14*(9), 2287. https://doi.org/10.3390/rs14092287

Kraus, K., & Pfeifer, N. (1998). Determination of terrain models in wooded areas with airborne laser Scanner Data. *ISPRS Journal of Photogrammetry & Remote Sensing*, *53* (4), 193–203. https://doi.org/10.1016/S0924-2716(98)00009-4

Lakens, D. (2017). Equivalence tests: A practical primer for t tests, correlations, and Meta-Analyses. *Social Psychological & Personality Science*, *8*(4), 355–362. https://doi.org/10.1177/1948550617697177

Leipe S C and Carey S K. (2021). Rapid shrub expansion in a subarctic mountain basin revealed by repeat airborne LiDAR. Environ. Res. Commun., 3(7), 071001 10.1088/2515-7620/ac0e0c

Li, X., Liu, C., Wang, Z., Xie, X., Li, D., & Xu, L. (2020). Airborne LiDAR: State-of-the-art of system design, technology and Application. *Measurement Science and Technology*, *32*(3), 032002. https://doi.org/10.1088/1361-6501/abc867

Liang, X., Kankare, V., Hyyppä, J., Wang, Y., Kukko, A., Haggrén, H., Yu, X., Kaartinen, H., Jaakkola, A., Guan, F., Holopainen, M., & Vastaranta, M. (2016). Terrestrial laser scanning in forest Inventories. *Isprs Journal of Photogrammetry & Remote Sensing*, *115*(mayo), 63–77. https://doi.org/10.1016/j.isprsjprs.2016.01.006

Liang, X., Wang, Y., Pyörälä, J., Lehtomäki, M., Yu, X., Kaartinen, H., Kukko, A., Honkavaara, E., Issaoui, A. E. I., Nevalainen, O., Vaaja, M., Virtanen, J.-P., Katoh, M., & Deng, S. (2019). Forest in situ observations using unmanned aerial vehicle as an alternative of terrestrial Measurements. *Forest Ecosystems*, *6*(1), 20. https://doi.org/10.1186/s40663-019-0173-3

Liu, X., & Zhang, Z. (2008). LiDAR data reduction for efficient and high quality DEM generation. XXI International Congress for Photogrammetry and Remote Sensing, Beijing, *37(Part B3b)*. In International Society for Photogrammetry and Remote Sensing edited by CHEN, Jun, JIANG, Jie, Jun. Beiging, China: The International Archives of the Photogrammetry, Remote Sensing and Spatial Information Sciences, pp. 173–178.

Liu, X., & Zhang, Z. (2011). Effects of LiDAR data reduction and breaklines on the accuracy of digital elevation Model. *Survey Review*, *43*(323), 614–628. https://doi.org/10.1179/003962611X13117748892317

Ma, Q., Su, Y., & Guo, Q. (2017). Comparison of canopy cover estimations from airborne LiDAR, aerial imagery, and satellite Imagery. *IEEE Journal of Selected Topics in Applied Earth Observations & Remote Sensing*, *10*(9), 4225–4236. https://doi.org/10.1109/JSTARS.2017.2711482

Medeiros, S., Hagen, S., Weishampel, J., & Angelo, J. (2015). Adjusting lidar-derived digital terrain models in coastal marshes based on estimated aboveground biomass Density. *Remote Sensing*, *7*(4), 3507–3525. https://doi.org/10.3390/rs70403507

Meng, X., Currit, N., & Zhao, K. (2010). Ground filtering algorithms for airborne LiDAR data: A review of critical Issues. *Remote Sensing*, *2*(3), 833–860. https://doi.org/10.3390/rs2030833

Miura, N., Yokota, S., Koyanagi, T. F., & Yamada, S. (2018). Herbaceous vegetation height map on riverdike derived from UAV LiDAR Data. *En* IGARSS, 2018 - 2018 IEEE International Geoscience and Remote Sensing Symposium, 5469–5472. https://doi.org/10.1109/IGARSS.2018.8517847

Novo, A., Fariñas-Álvarez, N., Martínez-Sánchez, J., González-Jorge, H., & Lorenzo, H. (2020). Automatic processing of aerial LiDAR data to detect vegetation continuity in the surroundings of Roads. *Remote Sensing*, *12*(10), 1677. https://doi.org/10.3390/rs12101677

Petrou, Z. I., Manakos, I., & Stathaki, T. (2015). Remote sensing for biodiversity monitoring: A review of methods for biodiversity indicator extraction and assessment of progress towards international Targets. *Biodiversity and Conservation*, *24*(10), 2333–2363. https://doi.org/10.1007/s10531-015-0947-z

Plowright, A. (2017). *_rFUSION: Tools for calling FUSION commands in R_. R package version 0.1.0. mayo de 2017*. https://rdrr.io/github/AndyPL22/rFUSION/

Raber, G. T., Jense, J. R., Schill, S. R., & Schuckman, K. (2002). Creation of digital terrain models using an adaptive lidar vegetation point removal Process. *Photogrammetric Engineering & Remote Sensing*, *68*(12), 1307–1315.

R Core Team. (2022). *R: A language and environment for statistical computing*. R Foundation for Statistical Computing. https://www.r-project.org/

Reddy, C. S. (2021). Remote sensing of biodiversity: What to measure and monitor from space to Species?. *Biodiversity and Conservation*, *30*(10), 2617–2631. https://doi.org/10.1007/s10531-021-02216-5

Rego, A., Cecilia, S. A. P., Cabo, C., Ordóñez, C., González, J. G. Á., Varela, R. A. D., & González, A. D. R. (2020). Reverse total shoulder arthroplasty for treatment of 3- and 4-part proximal humeral fractures: Clinical and radiological analysis with minimum follow-up of 2 years. *Geriatric Orthopaedic Surgery & Rehabilitation*, *11*. https://doi.org/10.3390/rs12223704

Riaño, D., Chuvieco, E., Ustin, S. L., Salas, J., Rodríguez-Pérez, J. R., Ribeiro, L. M., Viegas, D. X., Moreno, J. M., & Fernández, H. (2007). Estimation of shrub height for fuel-type mapping combining airborne LiDAR and simultaneous color infrared ortho Imaging. *International Journal of Wildland Fire*, *16*(3), 341. https://doi.org/10.1071/WF06003

Roussel, J.-R. 2023 *David Auty (reviews the documentation), Florian De Boissieu (fixed bugs and improved catalog features), Andrew Sánchez Meador (implemented wing2015() for segment_snags()), Bourdon Jean-François (contributed to Roussel2020() for track_sensor()), Gatziolis Demetrios (implemented Gatziolis2019() for track_sensor ()), Leon Steinmeier (contributed to parallelization management), y Stanislaw Adaszewski (Author of the C++ concaveman code). 2023. «lidR: Airborne LiDAR data manipulation and visualization for forestry Applications». 49*. https://cran.r-project.org/web/packages/lidR/index.html

Roussel, J.-R., Auty, D., Coops, N. C., Tompalski, P., Goodbody, T. R. H., Meador, A. S., Bourdon, J.-F., Boissieu, F. D., & Achim, A. (2020). LidR: An R package for analysis of airborne laser scanning (ALS) Data. *Remote Sensing of Environment*, *251*(diciembre), 112061. https://doi.org/10.1016/j.rse.2020.112061

Roussel, J.-R., Caspersen, J., Béland, M., Thomas, S., & Achim, A. (2017). Removing bias from LiDAR-based estimates of canopy height: Accounting for the effects of pulse density and footprint Size. *Remote Sensing of Environment*, *198*(septiembre), 1–16. https://doi.org/10.1016/j.rse.2017.05.032

Rowell, E., Seielstad, C., & Ottmar, R. (2015). Development and validation of fuel height models for terrestrial lidar – RxCADRE 2012. *International Journal of Wildland Fire*, *25* (enero). 1), 38. https://doi.org/10.1071/WF14170

Sevillano, I., Jesús, P.-R.-R., Díaz Varela, R. A., Martínez Sánchez, S., Pardo Gamundi, I., & Rodríguez Guitian, M. A. (2001). *Análisis y valoración de la Sierra de O Xistral: un modelo de aplicación de la Directiva Hábitat en Galicia*. Xunta de Galicia, Centro de Información e Tecnoloxía Ambiental.

Streutker, D. R., & Glenn, N. F. (2006). LiDAR measurement of sagebrush steppe vegetation Heights. *Remote Sensing of Environment*, *102*(1–2), 135–145. https://doi.org/10.1016/j.rse.2006.02.011

Su, J., & Bork, E. (2006). Influence of vegetation, slope, and lidar sampling angle on DEM Accuracy. *Photogrammetric Engineering & Remote Sensing*, *72*(noviembre), 1265–1274. https://doi.org/10.14358/PERS.72.11.1265

Torresan, C., Berton, A., Carotenuto, F., Gennaro, S. F. D., Gioli, B., Matese, A., Miglietta, F., Vagnoli, C., Zaldei, A., & Wallace, L. (2017). Forestry applications of UAVs in Europe: A Review. *International Journal of Remote Sensing*, *38*(8–10), 2427–2447. https://doi.org/10.1080/01431161.2016.1252477

Turner, W., Spector, S., Gardiner, N., Fladeland, M., Sterling, E., & Steininger, M. (2003). Remote sensing for biodiversity science and Conservation. *Trends in Ecology & Evolution*, *18*(6), 306–314. https://doi.org/10.1016/S0169-5347(03)00070-3

UN. (2009). *En* Guía para la Descripción de Suelos de la FAO. Capítulo 3: Factores de formación del suelo. (4ta ed. p. 12). División de Información. FAO. https://www.fao.org/3/a0541s/a0541s.pdf

Wallace, L., Lucieer, A., Watson, C., & Turner, D. (2012). Development of a UAV-LiDAR system with application to forest Inventory. *Remote Sensing*, *4*(6), 1519–1543. https://doi.org/10.3390/rs4061519

Wallace, L., Musk, R., & Lucieer, A. (2014). An assessment of the repeatability of automatic forest inventory metrics derived from UAV-Borne laser scanning Data. *IEEE Transactions on Geoscience & Remote Sensing*, *52*(11), 7160–7169. https://doi.org/10.1109/TGRS.2014.2308208

Warkentin, K., Stow, D., Uyeda, K., O'Leary, J., Lambert, J., Loerch, A., & Coulter, L. (2020). Shrub fractional cover estimation and mapping of San Clemente Island Shrubland Based on airborne multispectral imagery and lidar Data. *Remote Sensing*, *12*(21), 3608. https://doi.org/10.3390/rs12213608

Watt, M. S., Meredith, A., Watt, P., & Gunn, A. (2014). The influence of LiDAR pulse density on the precision of inventory metrics in young unthinned Douglas-fir stands during initial and subsequent LiDAR Acquisitions. *New Zealand Journal of Forestry Science*, *44*(1), 18. https://doi.org/10.1186/s40490-014-0018-3

Wieser, M., Hollaus, M., Mandlburger, G., Glira, P., & Pfeifer, N. (2016). Uls lidar supported analyses of laser

beam penetration from different als systems into vegetation. *ISPRS Annals of the Photogrammetry, Remote Sensing & Spatial Information Sciences*, *III-3*, 233–239. https://doi.org/10.5194/isprs-annals-III-3-233-2016

Wilkes, P., Lau, A., Disney, M., Calders, K., Burt, A., de Tanago, J. G., Bartholomeus, H., Brede, B., & Herold, M. (2017). Data acquisition considerations for terrestrial laser scanning of forest Plots. *Remote Sensing of Environment*, *196*(julio), 140–153. https://doi.org/10.1016/j.rse.2017.04.030

Zaque, B., William, L. K. E. R., & García, L. (2017). Obtención de parámetros óptimos en la clasificación de nubes de puntos LiDAR, a partir de sensores aerotransportados. *Avances Investigación en Ingeniería*, *14*(1), 9–20. https://doi.org/10.18041/1794-4953/avances.1.1280

Zhang, K., Shu-Ching Chen, D. W., Shyu, M.-L., Yan, J., Zhang, C., & Zhang, C. (2003). A progressive morphological filter for removing nonground measurements from airborne LIDAR data. *IEEE Transactions on Geoscience & Remote Sensing*, *41*(4), 872–882. https://doi.org/10.1109/TGRS.2003.810682

Zhang, W., Qi, J., Wan, P., Wang, H., Xie, D., Wang, X., & Yan, G. (2016). An easy-to-use airborne LiDAR data filtering method based on cloth Simulation. *Remote Sensing*, *8*(6), 501. https://doi.org/10.3390/rs8060501

Zhang, X., Bao, Y., Wang, D., Xin, X., Ding, L., Xu, D., Hou, L., & Shen, J. (2021). Using UAV LiDAR to extract vegetation parameters of inner Mongolian Grassland. *Remote Sensing*, *13*(4), 656. https://doi.org/10.3390/rs13040656

Zhao, X., Su, Y., Hu, T., Cao, M., Liu, X., Yang, Q., Guan, H., Liu, L., & Guo, Q. (2022). Analysis of UAV lidar information loss and its influence on the estimation accuracy of structural and functional traits in a meadow Steppe. *Ecological Indicators*, *135*(febrero), 108515. https://doi.org/10.1016/j.ecolind.2021.108515

Appendix A1

Table A1. R^2 and RMSE values obtained in different studies. Comparison of results.

Authors	Description	Sensor LiDAR	R^2	RMSE (m)
(Zhao et al., 2022)	Meadow steppe (China)	ULS Riegl VUX-1	0.17	0.40
(Curcio et al., 2022)	Salt marshes (Cadiz) h_{mean}	ULS DJI Zenmuse L1	<.10	0.12–0.18
(Leipe y Carey 2021)	Alpine and subalpine tundra (WCRB, Canada)	ULS RieglQ-780	0.79	0.44
(Hartley et al., 2020)	Young forest plantations (New Zealand)	ULS Snoopy V-Series	0.99	0.15
(Liang et al., 2019)	Boreal forest (Finland)	ULS Riegl VUX-1UAV	-	10–15%
(Miura et al., 2018)	Herbaceous vegetation on a levee (Japón)	ULS RIEGL VUX-1	0.79 $p < 0.01$	0.24
(Watt et al., 2014)	Young *Pseudotsuga menziesii* plantations (New Zealand)	ALS Optech ALTM 3100EA	0.85	1.01
(Riaño et al., 2007)	Heathland (Portugal) h_{max} (90_{th})	ALS Toposys II LiDAR system	0.48	0.18
(Su & Bork, 2006)	Grassland, tree, and shrub areas Gently sloping areas (Canada)	ALS Optech ALTM 2025	-	0.47
(Streutker y Glenn 2006)	Sagebrush steppe (Idaho)	ALS Optech ALTM 2025 LiDAR system.	0.72	-
(Rowell et al., 2015)	Forest stand (Florida)	TLS	0.70 $p \leq 0.0001$	-

Appendix B1: Distribution of returns in the ground filtering

Table B1. Distribution of returns in the ground filtering. Filter = ground classification filter as progressive morphological filter (PMF) & ground filter FUSION (GF).

					Percentage (%)	
Filter	Flight altitude	ID	Nº of ground returns	Density of ground returns (returns/m^2)	Ground returns	1st Return
PMF	80 m	d80_001	4.943.222	123,16	30%	98%
PMF	80 m	d80_002	4.953.223	123,41	30%	98%
PMF	80 m	d80_003	14.712.167	367,99	90%	99%
PMF	80 m	d80_004	16.143.857	401,67	99%	99%
PMF	80 m	d80_101	3.104.521	79,34	19%	97%
PMF	80 m	d80_102	3.725.380	93,28	23%	97%
PMF	80 m	d80_103	14.934.816	377,22	91%	99%
PMF	80 m	d80_104	16.129.937	401,32	98%	99%
PMF	80 m	d80_201	2.753.354	72,48	17%	97%
PMF	80 m	d80_202	3.419.115	86,40	21%	97%
PMF	80 m	d80_203	14.662.236	374,72	89%	99%
PMF	80 m	d80_204	16.122.115	401,13	78%	99%
PMF	100 m	d100_001	4.197.904	104,95	20%	98%
PMF	100 m	d100_002	4.899.593	122,12	24%	98%
PMF	100 m	d100_003	18.670.031	467,17	90%	99%
PMF	100 m	d100_004	20.438.803	508,48	99%	99%
PMF	100 m	d100_101	3.172.248	80,94	15%	98%
PMF	100 m	d100_102	3.759.299	94,09	18%	98%
PMF	100 m	d100_103	18.943.525	478,47	92%	99%
PMF	100 m	d100_104	20.423.969	508,11	99%	99%
PMF	100 m	d100_201	2.795.849	73,41	14%	98%
PMF	100 m	d100_202	3.462.127	87,52	17%	98%
PMF	100 m	d100_203	18.522.428	472,75	90%	99%
PMF	100 m	d100_204	20.414.670	507,88	99%	99%
GF	80 m	d80_r05	14.471.022	360,12	88%	99%
GF	80 m	d80_r1	13.407.693	333,66	82%	99%
GF	80 m	d80_r25	10.580.985	263,86	65%	98%
GF	80 m	d80_r5	8.303.130	212,25	51%	98%
GF	80 m	d80_r75	6.967.942	187,75	43%	98%
GF	80 m	d80_r10	6.316.812	185,20	39%	98%
GF	100 m	d100_r05	18.214.827	453,24	88%	99%
GF	100 m	d100_r1	18.214.827	453,24	88%	99%
GF	100 m	d100_r25	13.614.394	339,24	66%	99%
GF	100 m	d100_r5	10.625.882	270,30	51%	99%
GF	100 m	d100_r75	8.856.574	237,67	43%	99%
GF	100 m	d100_r10	7.932.105	232,48	38%	99%

Appendix B.2: Summary of Statistical Analysis

Table B2.1. Summary of tests conducted: DTM and CHM statistical analysis. PMF = progressive morphological filter, GF = *ground filter* Fusion; ID according to c[(flight height) _1st number (window size); 2nd & 3rd numbers (threshold height)] = c80_001.

	Flight Height	Filter	ID	Intercept	Slope	R2	RMSE
DTM	80	PMF	d80_001	1.951	0.999	0.9996	0.283
DTM	80	PMF	d80_002	3.317	0.996	0.9995	0.335
DTM	80	PMF	d80_003	0.166	1.001	0.9992	0.417
DTM	80	PMF	d80_004	−2.259	1.005	0.9991	0.445
DTM	80	PMF	d80_101	1.095	1.000	0.9997	0.255
DTM	80	PMF	d80_102	1.791	0.999	0.9997	0.268
DTM	80	PMF	d80_103	0.383	1.001	0.9992	0.408
DTM	80	PMF	d80_104	0.383	1.001	0.9992	0.408
DTM	80	PMF	d80_201	0.644	1.001	0.9997	0.250
DTM	80	PMF	d80_202	0.904	1.001	0.9997	0.255
DTM	80	PMF	d80_203	0.704	1.000	0.9993	0.404
DTM	80	PMF	d80_204	−2.151	1.005	0.9991	0.446
DTM	100	PMF	d100_001	1.930	0.999	0.9997	0.271
DTM	100	PMF	d100_002	3.084	0.997	0.9995	0.315
DTM	100	PMF	d100_003	−0.924	1.003	0.9992	0.411
DTM	100	PMF	d100_004	−2.718	1.006	0.9992	0.422
DTM	100	PMF	d100_101	0.536	1.001	0.9997	0.235
DTM	100	PMF	d100_102	1.342	1.000	0.9997	0.254
DTM	100	PMF	d100_103	0.004	1.001	0.9993	0.398
DTM	100	PMF	d100_104	−2.718	1.006	0.9992	0.422
DTM	100	PMF	d100_201	0.737	1.001	0.9998	0.230
DTM	100	PMF	d100_202	0.590	1.001	0.9997	0.245
DTM	100	PMF	d100_203	−0.056	1.001	0.9993	0.399
DTM	100	PMF	d100_204	−2.718	1.006	0.9992	0.422
DTM	80	GroundFilter	d80_r05	2.049	0.998	0.9994	0.369
DTM	80	GroundFilter	d80_r1	2.049	0.998	0.9994	0.369
DTM	80	GroundFilter	d80_r25	0.964	1.000	0.9996	0.285
DTM	80	GroundFilter	d80_r5	0.532	1.001	0.9997	0.273
DTM	80	GroundFilter	d80_r75	0.196	1.002	0.9996	0.302
DTM	80	GroundFilter	d80_r10	−0.823	1.004	0.9994	0.349
DTM	100	GroundFilter	d100_r05	2.942	0.996	0.9993	0.387
DTM	100	GroundFilter	d100_r1	2.870	0.997	0.9994	0.365
DTM	100	GroundFilter	d100_r25	1.744	0.999	0.9996	0.306
DTM	100	GroundFilter	d100_r5	1.149	1.000	0.9997	0.271
DTM	100	GroundFilter	d100_r75	0.487	1.001	0.9996	0.298
DTM	100	GroundFilter	d100_r10	0.144	1.002	0.9994	0.371
CHM	80	PMF	c80_001	0.860	0.584	0.3216	0.493
CHM	80	PMF	c80_002	0.999	0.495	0.2290	0.526
CHM	80	PMF	c80_003	1.229	0.338	0.0745	0.576
CHM	80	PMF	c80_004	1.289	0.237	0.0240	0.592
CHM	80	PMF	c80_101	0.758	0.631	0.3658	0.477
CHM	80	PMF	c80_102	0.799	0.624	0.3515	0.482
CHM	80	PMF	c80_103	1.212	0.379	0.0901	0.571
CHM	80	PMF	c80_104	1.212	0.379	0.0901	0.571
CHM	80	PMF	c80_201	0.736	0.635	0.3697	0.475
CHM	80	PMF	c80_202	0.746	0.648	0.3798	0.472
CHM	80	PMF	c80_203	1.201	0.400	0.1018	0.568
CHM	80	PMF	c80_204	1.290	0.234	0.0238	0.592
CHM	100	PMF	c100_001	0.609	0.770	0.4380	0.449
CHM	100	PMF	c100_002	0.731	0.707	0.3628	0.478
CHM	100	PMF	c100_003	1.114	0.509	0.1206	0.562
CHM	100	PMF	c100_004	1.114	0.509	0.1206	0.562
CHM	100	PMF	c100_101	0.474	0.835	0.5019	0.423
CHM	100	PMF	c100_102	0.530	0.821	0.4752	0.434
CHM	100	PMF	c100_103	1.083	0.570	0.1497	0.552
CHM	100	PMF	c100_104	1.162	0.470	0.0624	0.580
CHM	100	PMF	c100_201	0.456	0.829	0.5135	0.418
CHM	100	PMF	c100_202	0.488	0.829	0.4937	0.426
CHM	100	PMF	c100_203	1.086	0.563	0.1463	0.553
CHM	100	PMF	c100_204	1.162	0.470	0.0624	0.580
CHM	80	GroundFilter	c80_r05	1.171	0.416	0.1231	0.561
CHM	80	GroundFilter	c80_r1	1.171	0.416	0.1231	0.561
CHM	80	GroundFilter	c80_r25	0.970	0.579	0.2927	0.504
CHM	80	GroundFilter	c80_r5	0.916	0.575	0.3058	0.499
CHM	80	GroundFilter	c80_r75	0.888	0.581	0.3262	0.492
CHM	80	GroundFilter	c80_r10	0.934	0.535	0.2700	0.512
CHM	100	GroundFilter	c100_r05	1.175	0.397	0.1339	0.557
CHM	100	GroundFilter	c100_r1	1.119	0.453	0.1855	0.541
CHM	100	GroundFilter	c100_r25	0.991	0.546	0.2731	0.511
CHM	100	GroundFilter	c100_r5	0.901	0.581	0.3166	0.495
CHM	100	GroundFilter	c100_r75	0.848	0.609	0.3480	0.484
CHM	100	GroundFilter	c100_r10	0.928	0.515	0.2644	0.514

Table B2.2. Statistics, NMAD, RMSE, and R^2 for the alternative yielding superior results in ground point filtering (d100_201) according to different DTM raster resolutions.

		Resolution			
Raster Type	Statistic	0.10 m	0.25 m	0.50 m	1 m
DTM	NMAD	0.203	0.205	0.203	0.230
DTM	RMSE	0.244	0.242	0.230	0.234
DTM	R^2	0.9998	0.9998	0.9998	0.9998

Statistics, NMAD, RMSE, and r_s for the optimal performance of DTM raster resolution (0.5m) according to different CHM raster resolutions

		Resolution	
Raster Type	Statistic	0.10 m	0.25 m
CHM	NMAD	0.350	0.291
CHM	RMSE	0.424	0.419
CHM	R^2	0.476	0.514